MNRAS **000**, 000–000 (0000) Preprint 31 March 2017 Compiled using MNRAS LATEX style file v3.0

A 1.4 deg^2 blind survey for CII], CIII] and CIV at z ∼ 0.7 − 1.5. I: nature, morphologies and equivalent widths

Andra Stroe[1⋆†], David Sobral[2,3], Jorryt Matthee[2], João Calhau[3], Ivan Oteo[4,1]
[1]*European Southern Observatory, Karl-Schwarzschild-Str. 2, 85748, Garching, Germany*
[2]*Leiden Observatory, Leiden University, P.O. Box 9513, NL-2300 RA Leiden, The Netherlands*
[3]*Department of Physics, Lancaster University, Lancaster, LA1 4YB, UK*
[4]*Institute for Astronomy, University of Edinburgh, Royal Observatory, Blackford Hill, Edinburgh EH9 3HJ UK*

31 March 2017

ABSTRACT

While traditionally associated with active galactic nuclei (AGN), the properties of the CII], CIII] and CIV emission lines are still uncertain as large, unbiased samples of sources are scarce. We present the first blind, statistical study of CII], CIII] and CIV emitters at $z \sim 0.68, 1.05, 1.53$, respectively, uniformly selected down to a flux limit of $\sim 4 \times 10^{-17}$ erg s^{-1} cm^{-1} through a narrow band survey covering an area of ~ 1.4 deg^2 over COSMOS and UDS. We detect 16 CII], 35 CIII] and 17 CIV emitters, whose nature we investigate using optical colours as well as *HST*, X-ray, radio and far infra-red data. We find that $z \sim 0.7$ CII] emitters are consistent with a mixture of blue (UV slope $\beta = -2.0 \pm 0.4$) star forming galaxies with disky *HST* structure and AGN with Seyfert-like morphologies. Bright CII] emitters have individual X-ray detections as well as high average black hole accretion rates (BHAR) of $\sim 0.1\ M_\odot$ yr^{-1}. CIII] emitters at $z \sim 1.05$ trace a general population of SF galaxies, with $\beta = -0.8 \pm 1.1$, a variety of optical morphologies, including isolated and interacting galaxies and low BHAR ($< 0.02\ M_\odot$ yr^{-1}). Our CIV emitters at $z \sim 1.5$ are consistent with young, blue quasars ($\beta \sim -1.9$) with point-like optical morphologies, bright X-ray counterparts and large BHAR ($0.8\ M_\odot$ yr^{-1}). We also find some surprising CII], CIII] and CIV emitters with rest-frame equivalent widths which could be as large as $50 - 100$ Å. AGN or spatial offsets between the UV continuum stellar disk and the line emitting regions may explain the large EW. These bright CII], CIII] and CIV emitters are ideal candidates for spectroscopic follow up to fully unveil their nature.

Key words: galaxies: high redshift, star formation, active, quasars: emission lines, cosmology: observations

1 INTRODUCTION

Rest-frame ultra-violet (UV) emission lines are of great importance for extragalactic astrophysics as they can be used to infer gas metallicities, temperatures and the strength of the ionising field (e.g. Shapley et al. 2003; Osterbrock & Ferland 2006). Observing these lines in the local Universe is challenging. However, for galaxies at large cosmic distances the rest-frame UV emission lines are redshifted into the easily observable optical range. Historically rest-frame UV spectra were mainly used to spectroscopically confirm UV-bright galaxies at $z \gtrsim 3$ selected through the Lyman Break technique (Lyman Break galaxies, LBG, Steidel et al. 1996; Lowenthal et al. 1997). In the last 15 years, strong rest-frame UV lines have been discovered in a variety of galaxies at $z > 1$, which could be used to constrain the physics in high-redshift counterparts of local galaxies (Best et al. 2000; Shapley et al. 2003; Erb et al. 2010; Rigby et al. 2015).

Intrinsically the brightest rest-frame UV line is Lyα, which is produced in HII regions as well as in galaxies with an active galactic nucleus (AGN) (e.g. Ouchi et al. 2008; Nilsson et al. 2009; Cowie et al. 2010; Hayes 2015; Matthee et al. 2016, 2017; Sobral et al. 2017). However, it is difficult to interpret observations of Lyα, as the line is scattered by neutral hydrogen and easily absorbed by dust (e.g. Dijkstra 2014; Hayes 2015). The amount of Lyα that escapes a galaxy therefore depends on the properties of the interstellar medium.

Other UV lines, such as CII], CIII] and CIV (Table 1) have recently been explored as they can be relatively bright compared to Lyα and can be used either individually or in combination to constrain the physics of the host galaxy. CIII] (ionisation potential of 24.4 eV, Veilleux 2002), for example, was found to be the strongest UV line after Lyα in stacks of LBGs at $z \sim 3$ (Shapley et al. 2003) and about 10 per cent of the observed strength of Lyα in

⋆ E-mail: astroe@eso.org
† ESO Fellow

Table 1. Line emitters studied in this work, with rest-frame wavelength, ionisation energy χ (Veilleux 2002), luminosity distance D_L and redshift range traced by the NB392 filter, with central wavelength 3919 Å and FWHM of 52 Å. The sample is drawn from the emission line catalogue presented in Sobral et al. (2017), which focuses on selection and properties of Lyα emitters at $z \sim 2.2$.

Line	λ_{line} (Å)	χ (eV)	z_{line} at FWHM	D_L (10^3 Mpc)	Comments
CII]	2326	11.3	0.673 – 0.696	4.14	likely traces shocks around AGN
CIII]	1907, 1909	24.4	1.039 – 1.066	7.04	produced in SF and BLR of AGN
CIV	1549, 1551	47.9	1.513 – 1.546	11.47	likely produced in BLR of AGN or in gas around very massive stars

faint, lensed galaxies at $1.5 < z < 3$ (Stark et al. 2014). CIV (47.9 eV) is also a bright UV line, with a typical ratio of just below one with CIII] (e.g. Gutkin et al. 2016; Feltre et al. 2016).

High ionisation rest-frame UV emission lines of Carbon were originally thought to originate from close to the AGN engine as they require a strong radiation field and high temperatures. CIII] is a high-ionisation, intercombination doublet (1907, 1909 Å) expected to be mostly produced in the outer parts of the broad line region (BLR) of the AGN (Osterbrock & Ferland 2006). However, at $z \sim 2-3$, CIII] emitters are also found in star forming (SF) galaxies and trace a slightly sub-solar metallicity, a high ionization parameter and a hard radiation field (Rigby et al. 2015; Bayliss et al. 2014). Photoionisation models presented in Jaskot & Ravindranath (2016) indicate that CIII] can be produced in starburst galaxies and is the strongest line (with $\lambda < 2700$ Å) after Lyα.

UV collisionally excited lines such as CII] and CIV are stronger in very high temperature regions ($2 \times 10^4 - 10^5$ K) in the cooling region behind shocks around the AGN than in areas with lower temperature such as those that can be reached with photoionisation (10^4 K, Osterbrock & Ferland 2006; Allen et al. 1998). CII] and CIV are therefore expected to be more strongly produced in AGN hosting galaxies. Indeed, Baldwin (1977) found a correlation between the strength of the resonant CIV (1548, 1551 Å) line and the continuum luminosity, indicating that the line emitting gas is located very close to the ionisation source. While traditionally associated with BLR emission, CIV was found to be correlated with gas temperature and an intense radiation field (Osterbrock & Ferland 2006), such as the one caused by AGN or by massive stars after a recent SF episode (Stark et al. 2014; Mainali et al. 2016; Schmidt et al. 2017). In a study of radio galaxies, De Breuck et al. (2000) noted that CII] is five times more sensitive to shock ionisation than high ionisation UV lines, such as CIV. Therefore, there is compelling evidence that the semi-forbidden CII] (11.3 eV, Veilleux 2002) line traces shocks and in combination with other lines is effective in determining the power source of ionisation (Best et al. 2000, 2002).

While independently CII], CIII] and CIV trace gas metallicity and electron density, in combination they can be used as estimators which are, to first order, independent of abundance, metallicity and dust-extinction (Best et al. 2002). Therefore, CII], CIII] and CIV line ratios are some of the best diagnostics to separate excitation by fast shocks and photoionisation in a hard photon spectrum (Allen et al. 1998).

Given their relative strength to Lyα, CIII] and CIV have been proposed as a good avenue for spectroscopically confirming high redshift galaxies (Stark et al. 2014, 2015a,b), particularly within the epoch of reionisation, when Lyα scattering is expected to increase leading to a significant decrease of surface brightness. As a result, in recent years, targeted searches for CIII] and CIV emitters at high redshift have emerged. For example, Rigby et al. (2015) detect CIII] in 11 $z \sim 1.6-3$ lensed galaxies, and Bayliss et al. (2014) find strong CIII] in a $z \sim 3.63$ lensed starburst. Stark et al. (2015a) present tentative detections of CIII] in two galaxies at $z > 6$, while Ding et al. (2016) detect CIII] in one galaxy at $z \sim 5.7$. By contrast, Zitrin et al. (2015a) do not obtain a detection of CIII] in a sample of 7 $z \sim 7-8$ photometric candidates. Very recently, Du et al. (2016) presented a spectroscopic study of a sample of continuum selected CIII] emitters at $z \sim 1$. With a detection rate of ~ 20 per cent, their CIII] emitters have much lower EW (1.3 Å) than higher redshift examples. Du et al. (2016) also found that the stronger EW sources appear in fainter, bluer and lower-mass galaxies. Schmidt et al. (2017) and Mainali et al. (2016) obtain a detection of CIV in a multiply-lensed $z = 6.1$, Lyα-emitting SF galaxy, but without a CIII] detection. Despite the growing number of detections, the samples of CIII] and CIV emitters suffer from selection biases (e.g. spectroscopically selected, lensed sources, redshift known from Lyα).

Despite the potential importance of CII], CIII] and CIV for understanding AGN physics and the nature of stellar populations at high redshift, not much is known about these emitters in a statistical sense, as no blind studies have been performed. As such, the nature, number densities and EW distributions are largely unknown. We seek to improve our understanding of CII], CIII] and CIV emitters by performing the first blind survey of these lines, without any preselection in terms of Lyα or UV properties. Our sample is uniformly selected down to a flux of $\sim 4 \times 10^{-17}$ erg s^{-1} cm^{-2}, in three redshift slices around $z \sim 0.7$, ~ 1.0, ~ 1.5 for CII], CIII] and CIV, respectively. The limiting observed EW is 16 Å and the limiting U magnitude is ~ 26.5. The sources were discovered by exploring the ~ 1.4 deg^2 CAlibrating LYMan-α with Hα NB survey (CALYMHA, Matthee et al. 2016; Sobral et al. 2017) over the COSMOS and UDS fields.

Our results are presented in two parts. In this paper (Paper I), we use the emission line data in combination with multiwavelength observations in the optical, radio, X-ray and far infra red (FIR) to unveil the characteristics of individual CII], CIII] and CIV emitters selected with the CALYMHA survey. We study the likely physical origin of the emission lines and how their properties compare with AGN and SF galaxies at similar redshifts. In the companion paper (Paper II, Stroe et al. 2017b) we investigate the statistical properties of the CII], CIII] and CIV emitters through luminosity functions (LF) and obtain the volume-average line ratios relative to e.g. Lyα and Hα.

We organise the paper as follows: in Section 2 we present the CALYMHA parent sample, while in Section 3 we select the CII], CIII] and CIV emitters. We discuss the colour and EW properties of the emitters as well as their Hubble Space Telescope (*HST*), radio, far infra-red (FIR) and X-ray properties in Section 4. The interpretation of our results and the implication for the physics CII], CIII]

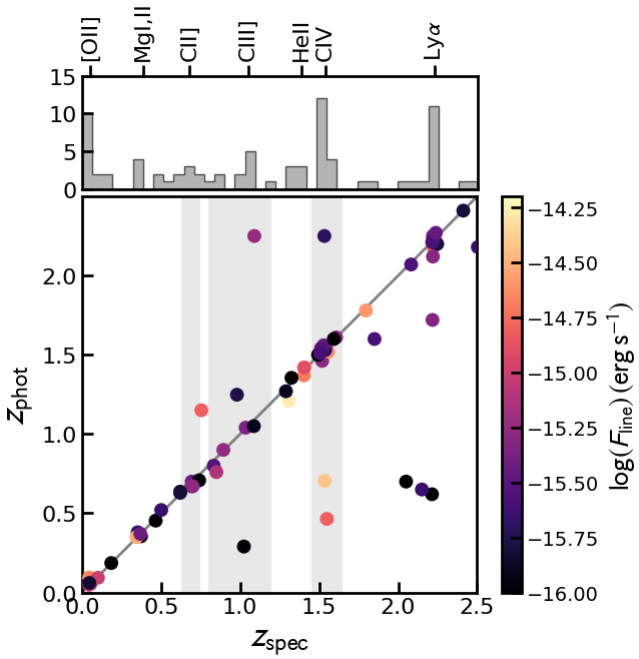

Figure 1. Photometric versus spectroscopic redshift for our NB392 line emitters, using data from e.g. Ilbert et al. (2009), Cirasuolo et al. (2010) and Lilly et al. (2009), as well as our own X-SHOOTER Very Large Telescope follow-up. The grey shaded areas indicate the redshift ranges where the NB filter is sensitive to CII], CIII] and CIV. The top panel shows the distribution of spectroscopic redshifts, where we also mark the main emission lines picked up by the NB filter.

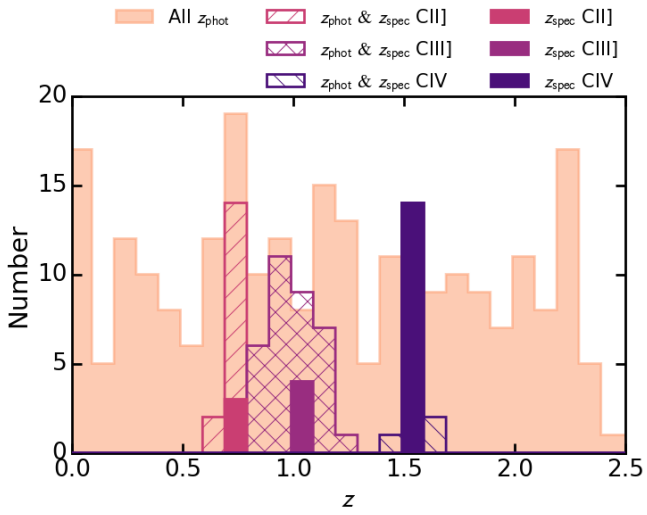

Figure 2. Histogram of all photometric redshifts, focusing on CII], CIII] and CIV. Note the narrow ranges chosen for selection of sources based on photometric redshifts, ensuring that low redshift ($z < 0.4$) emitters such as [OII], [NeV], MgI and MgII are rejected.

and CIV production can be found in Section 5, with conclusions and outlook in Section 6.

Throughout the paper, we use a flat ΛCDM cosmology ($H_0 = 70\,\mathrm{km\,s^{-1}\,Mpc^{-1}}$, $\Omega_M = 0.3$, $\Omega_\Lambda = 0.7$), and perform calculations with the aid of the Wright (2006) cosmology calculator. All magnitudes are in the AB system and we use a Chabrier (2003) initial mass function (IMF).

2 SURVEY DESCRIPTION

We use the CALYMHA sample of emission line galaxies to select CII] ($z \sim 0.63$), CIII] ($z \sim 1.05$) and CIV ($z \sim 1.53$) line emitters in the COSMOS and UDS fields. The CALYMHA survey design, observations and data reduction is presented in full in Sobral et al. (2017) and here we give a brief summary of the survey strategy and goals. The programme surveyed a combined area of ~ 1.4 deg^2 in the COSMOS and UDS fields using a narrow band (NB) filter (NB392, central wavelength $\lambda_C = 3918$ Å and width $\Delta\lambda = 52$ Å) mounted on the Isaac Newton Telescope[1]. The NB filter was designed to select line emitters, with a particular focus on Lyα emitters at $z \sim 2.23$, and cross-match them with Hα galaxies at the same redshift (Sobral et al. 2013). The main goal of the survey is to unveil the nature of Lyα emitter by studying the luminosity function (LFs) and determining Lyα escape fractions as function of galaxy properties both for Hα and Lyα selected samples at $z \sim 2.2$ (Matthee et al. 2016; Sobral et al. 2017).

The CALYMHA COSMOS+UDS survey selected a total of 440 line emitters down to a 3σ line flux limit of $\sim 4 \times 10^{-17}$ erg s^{-1} cm^{-2}, down to an observed EW limit of 16 Å. Based on spectroscopic and photometric redshifts, the emitter population contains a significant fraction of CII], CIII] and CIV emitters (Sobral et al. 2017), thus rendering CALYMHA an ideal sample to study these emitters in a statistical, unbiased way with a clear selection function. Given the width of the NB filter and their rest-frame wavelength, the line emitters are traced over a narrow redshift range (see Table 1).

2.1 Ancillary data

In addition to the CALYMHA NB and *U* band data, we use ancillary spectroscopic and photometric redshifts and photometry from the COSMOS and UDS surveys (Capak et al. 2007; Lawrence et al. 2007; Ilbert et al. 2009; Laigle et al. 2016). About 40 per cent of our sources are faint in the *i* and *K* bands or are located in masked regions and are thus not included in the publicly available COSMOS and UDS catalogues. There are 80 emitters with spectroscopic redshifts, most of which also have a photometric redshift (Fig. 1, data from Yamada et al. 2005; Simpson et al. 2006; van Breukelen et al. 2007; Geach et al. 2008; Ouchi et al. 2008; Smail et al. 2008; Lilly et al. 2009; Ono et al. 2010). However, in 10 cases, only a spectroscopic redshift is available. We also include the redshifts derived by Sobral et al. (2017) from dual, triple and quadruple detection of emission lines in NB filters. These very precise photometric redshifts have accuracies close to a spectroscopic measurement. The total tally for sources with redshifts (spectroscopic or photometric) is 269, or 61 per cent of the total number of emitters.

We also explore the deep, publicly available *HST* data in the F814W filter (Koekemoer et al. 2007; Massey et al. 2010), *Chandra* space telescope X-ray observations (Elvis et al. 2009), FIR *Herschel* data (Oliver et al. 2012) and radio Very Large Array images at 1.4 GHz (Schinnerer et al. 2004, 2010) in the COSMOS field to further investigate the nature of the line emitters. We employ direct detections as well as stacking techniques for this purpose. We note that the Chandra deep data is only available in a sub-area of the COSMOS field, hence only a fraction of the sources will have

[1] http://www.ing.iac.es/Astronomy/telescopes/int/

Table 2. Criteria for selecting a source as a CII], CIII] or CIV emitter. The z_{spec} ranges used correspond to the full transmission range covered by the NB filter. Note that we are using conservative z_{phot} cuts to minimise contamination. Sources selected as Lyα by Sobral et al. (2017) using colour-colour selections were removed from the sample. The number of sources of each type, selected based on z_{spec} and additional z_{phot} are also listed.

Line	z_{spec} selection range	z_{spec} sources	z_{phot} selection range (sources without z_{spec})	z_{phot} sources	All
CII]	0.661 – 0.707	3	0.63 – 0.75	13	16
CIII]	1.025 – 1.080	4	0.8 – 1.2	30	34
CIV	1.486 – 1.563	14	1.4 – 1.7	3	17

counterparts and/or coverage. The UDS field is partly covered with *HST* data as part of the CANDELS survey (Koekemoer et al. 2011).

3 SELECTING CII], CIII] AND CIV EMITTERS

In order to select CII], CIII] and CIV emitters at the redshifts traced by the NB392 filter, we use a combination of spectroscopic and photometric redshifts.

3.1 Redshifts

For the COSMOS field, Ilbert et al. (2009) derived photometric redshifts using a range of templates, including star, galaxy and quasar templates for an *i* band selected sample. Blindly using the galaxy templates results in large discrepancies between the chosen photometric redshift and the true redshift, when spectroscopy is available. Keeping in mind that a fraction of CII], CIII] and CIV emitters is possibly tracing AGN activity, we expect in many cases the quasar templates to perform better. Ilbert et al. (2009) also provide the χ^2 for the best fit stellar, galaxy and quasar template. We found that simply choosing the template which provided the lowest χ^2 fit worked well: for the sources with both z_{phot} and z_{spec}, the two estimates matched (see Fig. 1). When choosing the best z_{phot} estimate based on χ^2, 88 per cent of the photometric redshifts are within 0.1 of the spectroscopic ones. In cases where neither template was a good fit (high $\chi^2 > 100$), all photometric redshift estimates were catastrophically off.

We also tested the new COSMOS z_{phot} catalogue presented in Laigle et al. (2016) using the same method of selecting the best template (minimising the χ^2), but found that the Ilbert et al. (2009) photometric redshifts correlate better with the spectroscopic redshifts in our sample. Laigle et al. (2016) is selected in the near infrared and Ilbert et al. (2009) in the optical. Since our sources are optically selected (in the very blue), it is maybe unsurprising Ilbert et al. (2009) z_{phot} work better, given their weighting towards optical bands. In the case of UDS, a single photometric redshift estimate is available (Cirasuolo et al. 2010).

Overall, for the entire sample, 84 per cent of photometric redshifts are within 0.1 of the spectroscopic redshift (Fig. 1). The sample is however not spectroscopically complete, especially for fainter sources, so the photometric redshift accuracy derived here is not necessarily applicable for all the sources without a spectroscopic redshift (Fig. 2).

3.2 Final selection criteria

For a source to make the CII], CIII] or CIV emitter selection, we first remove all sources selected as Lyα by Sobral et al. (2017). It then has to fulfill at least one of the criteria listed below. We summarise the criteria in Table 2 and describe them below:

- A spectroscopic redshift within the range probed by the respective filter, within two FWHM. We choose this wider range since the filter transmission drops slowly towards its wavelength edges, effectively being sensitive to emitters at twice the FWHM. This also accounts for broad lines.
- If spectroscopy is not available, we select a source if is has a photometric redshift within ~ 0.2 of the redshift range the NB filter is sensitive to. Note our very conservative cuts are chosen to maximise the purity of the sample.

The redshift distribution of sources selected as CII], CIII] and CIV is shown Fig. 2. The narrow photometric redshift ranges chosen for selection ensures that we do not include bright, low redshift emitters such as [OII] at $z \sim 0.05$, [NeV] at $z \sim 0.15$ and MgI and MgII at $z \sim 0.4$ in our sample. Our photometric redshift selection is conservative as there could be sources with z_{phot} in the $1.2 - 1.4$ range which could be either CIII] or CIV (Fig. 2).

Sobral et al. (2017) used *BzK* colour selections to further improve the completeness of their Lyα sample and thus include some sources with lower photometric redshifts. If we did not remove the Lyα selected sources, we would select an extra 9 CIII] and 16 CIV sources. We remove sources selected as Lyα by Sobral et al. (2017) to ensure a high purity and obtain conservative, but secure samples. Note however, the highly unusual colours of CIV emitters (see Section 4.1), which means that some real CIV emitters might have been selected as Lyα and thus were removed from our sample. Spectroscopic follow up is required to further investigate this. See also discussion in Sobral et al. (2017) on the removal of the vast majority of CIII] and CIV contaminants in CALYMHA, which is usually not done in other Lyα surveys.

4 PROPERTIES OF THE CII], CIII] AND CIV SAMPLES

Table 2 lists the final samples of CII], CIII] and CIV emitters, which include spectroscopically confirmed sources and sources selected through their z_{phot}. We have 3 spectroscopically confirmed CII] emitters in addition to 13 z_{phot}. In the case of CIII] emitters, we have 4 spectroscopically selected sources and 30 with z_{phot}. We obtain 14 CIV sources with z_{spec} and 3 with z_{phot}. Note the particularly high spectroscopic completeness of the CIV sample, a likely result of the follow up of Chandra COSMOS sources.

In this section, we study the colour-colour properties as well as the colour and EW distributions with the aim of investigating the nature of the CII], CIII] and CIV emitters, as well as test the robustness of our sample. We also investigate the properties of the emitters using X-ray, radio and space telescope optical data. Tables 3 and 4 summarise the EW, UV, optical, X-ray and radio properties of the sample, while Tables B1, B2 and B3 describe individual CII], CIII] and CIV emitters. We list their sky coordinates, line luminosity, rest-frame EW_{rest}, observed $(U-B)_{obs}$ colours and describe their optical *HST* morphologies, and their X-ray and/or radio

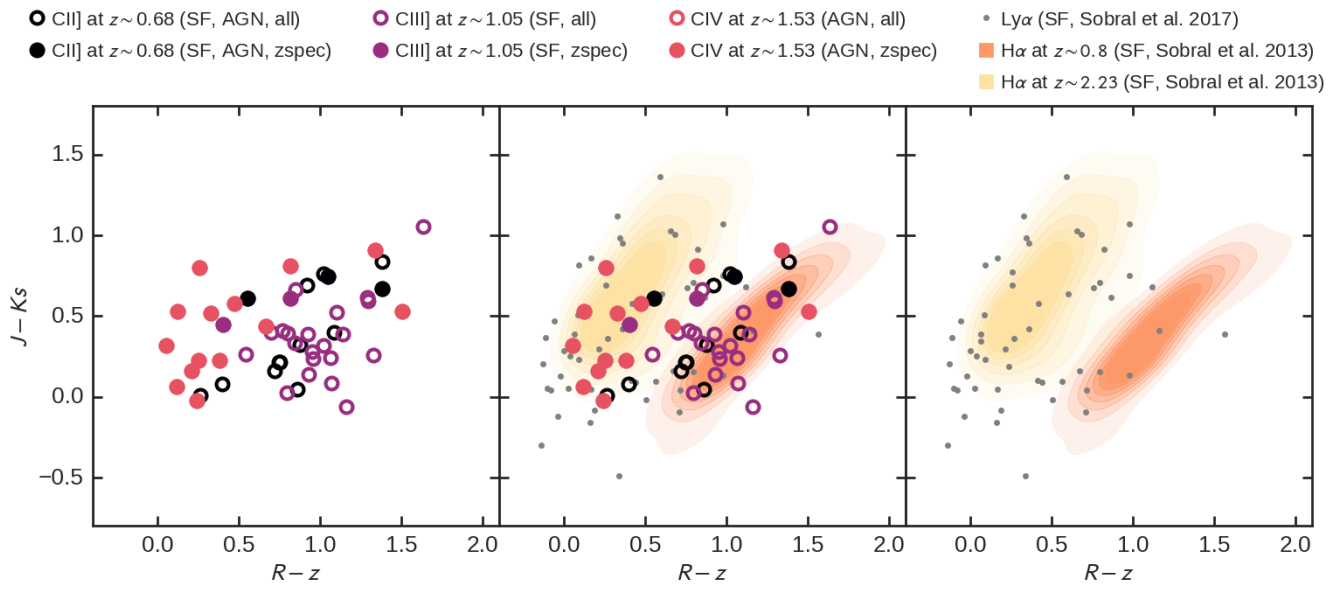

Figure 3. $R-z$ versus $J-Ks$ colour-colour plot for the emitters. Lyα emitters at $z \sim 2.23$ from the CALYMHA survey (Sobral et al. 2017) and Hα emitters from the HiZELS project (Sobral et al. 2013) are also plotted. CII] and CIII] emitters are located in the $z \sim 0.8 - 1.5$ SF galaxy regime. However, the CIV emitters have unusual colours, following the distribution of SF at $z \sim 2.23$, rather than 1.5.

counterparts. Note that while most of the COSMOS part of the CALYMHA survey is covered by *HST* and VLA radio data, the deep Chandra data is only available for a sub-area. In the case of UDS, only *HST* data is available and for a small subarea of the field.

To describe the properties of our CII], CIII] and CIV sources, we will use the emission line luminosity, which is derived from the observed flux measured within 3″ apertures (which corresponds to about 30 kpc at the redshift of our emitters, see also Sobral et al. 2017):

$$L_{\rm line} = 4\pi D_L^2(line) F_{\rm line}, \quad (1)$$

where line is CII], CIII] or CIV and $D_L(line)$ is the luminosity distance at the redshift of each line (see Table 1).

4.1 Colour-colour properties

In SF galaxies, the $R-z$ versus the $J-Ks$ colour space probes the 4000 Å break, which moves from between the R and z filters for sources at $z \sim 0.7 - 1.2$, to between J and Ks for sources at $z > 2.1$. In Fig. 3, this is illustrated by the population of SF Hα emitters from Sobral et al. (2013) which move from the lower-right side at $z \sim 0.8$ (large $R-z$, small $J-Ks$) of the plot towards the upper-right side (small $R-z$, larger $J-Ks$) at $z \sim 2.2$. For comparison, we also overplot the CALYMHA Lyα emitters at $z \sim 2.2$.

Some CII] emitters at $z \sim 0.7$ are located in the colour space of SF galaxies at $z \sim 1.5$, so they have atypical colours for their redshift, indicating that while some may trace SF galaxies, some, as expected, probably result from ionisation in AGN through shocks.

CIII] sources mostly lie in the region of $z \sim 0.8 - 1.0$ SF galaxies, possibly indicating a SF, rather than AGN nature of these emitters. Note that the most extreme CIII] emitter, with a very low $R-z$ colour, is an AGN (see Section 4.6) and the most luminous in the emission line ($\sim 10^{42.4}$ erg s^{-1}).

Given the large ionisation energy necessary to produce CIV, it is expected that CIV requires either an AGN or very hot stars. It is therefore perhaps not surprising that most CIV emitters at $z \sim 1.5$ do not have colours consistent with SF galaxies at that redshift, but lie in the region of $z \sim 2.2$ Lyα emitters. Note that all CIV sources with all the two colours required for Fig. 3 are spectroscopically confirmed, so the unusual colours cannot be attributed to a wrong selection. It is therefore crucial to consider the contamination by CIV emitters to samples of NB selected Lyα emitters: without redshifts, when using colours, many lower redshift CIV sources will be confused with higher redshift Lyα emitters, as noted by Sobral et al. (2017). CIV have unusual spectral shapes in other bands as well. For example, the criteria Konno et al. (2016) used for selecting Lyα emitters at $z \sim 2.2$ ($(U-NB) > 0.5$ and $(B-NB) > 0.2$), would select 7 spectroscopically confirmed CIV emitters as Lyα emitters. Note this corresponds to half the sample of confirmed CIV emitters. Even when using the criteria defined by Konno et al. (2016) to select 'secure' Lyα emitters ($(U-NB) > 0.9$ and $(B-NB) > 0.2$), we would still select 5 spectroscopically confirmed CIV into a Lyα sample. These CIV emitters are typically luminous, so they result in contamination of the bright end of the Lyα distribution (Sobral et al. 2017; Matthee et al. 2017). Because this contamination is mostly at bright fluxes, it is less important in deep but small area NB surveys (e.g. Trainor et al. 2015).

4.2 Observed and rest-frame $U-B$ colours

Fig. 4 displays the distribution of observed $(U-B)_{\rm obs}$ colours for our emitters, while the mean and median colours are listed in Table 3. For individual sources, the numbers are listed in Tables B1, B2 and B3. At $z \sim 0.7 - 1.5$, $(U-B)_{\rm obs}$ approximately traces the rest-frame UV. Note that all but 2 CIII] emitters have both U and B measurements. Note however that U is contaminated by the emission line, thus the colours should be interpreted with caution. The $(U-B)_{\rm obs}$ corresponds to approximately:

- CII]: short and long side of restframe *NUV*
- CIII]: restframe *NUV* and *FUV*
- CIV: short and long side of restframe *FUV*

Table 3. Rest-frame $EW_{\rm rest}$, observed $(U-B)_{\rm obs}$ and UV slope β of the emitters which have photometric or spectroscopic redshifts. We also list the observed filters used for tracing the rest-frame UV. Note that the rest-frame wavelength traced for calculating the β slopes vary slightly depending on the emitter type. See Section 4.3 for more details. The uncertainties reported represent the standard deviation of the sample.

Line	$z_{\rm spec}$	Mean $EW_{\rm rest}$ (Å)	Median $EW_{\rm rest}$ (Å)	Mean $(U-B)_{\rm obs}$ (mag)	Median $(U-B)_{\rm obs}$ (mag)	Mean β	Median β	Filters for β slope
CII]	0.68	82 ± 56	74 ± 70	0.25 ± 0.20	0.26 ± 0.25	-2.0 ± 0.4	-1.9 ± 0.5	*NUV*, *U*
CIII]	1.05	93 ± 59	87 ± 74	0.25 ± 0.37	0.21 ± 0.46	-0.8 ± 1.1	-0.6 ± 1.4	*U*, *B*
CIV	1.53	51 ± 46	34 ± 58	0.15 ± 0.37	0.21 ± 0.46	-1.9 ± 0.8	-1.6 ± 1.0	*U*, *V*
Lyα	2.23	85 ± 57	77 ± 71	0.18 ± 0.25	0.23 ± 0.31	-1.6 ± 0.6	-1.7 ± 0.7	*g*, *R*
Hα	2.23					-1.0 ± 0.6	-1.0 ± 0.7	*g*, *R*

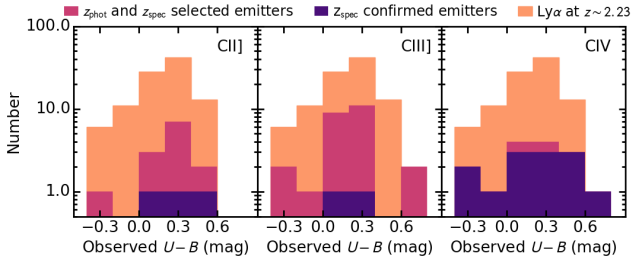

Figure 4. Distribution of observed $(U-B)_{\rm obs}$ colours of the emitters. The distribution of the Lyα emitters at $z\sim2.23$ (Sobral et al. 2017) is given for reference. The $(U-B)_{\rm obs}$ average for the C emitters at $0.7\lesssim z\lesssim1.5$ indicate blue colours, consistent with Lyα emitters at $z\sim2.23$.

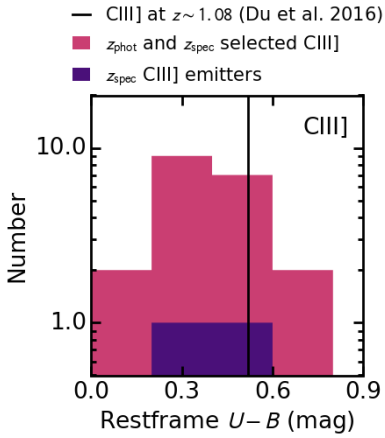

Figure 5. Distribution of rest-frame $(U-B)_{\rm rest}$ colours (observed $i-z$ colours) of the CIII] emitters. The rest-frame $(U-B)_{\rm obs}$ from Du et al. (2016) averages are only slightly larger, but consistent with our results. This shows that our CIII] emitters are a relatively blue population of sources, but that our blind selection may also be recovering a few sources which are even bluer than the average.

All three types of emitters studied in this paper have relatively blue colours with mean $(U-B)_{\rm obs}$ colours in the $0.15-0.25$ range. Our emitters are consistent in colour to Lyα emitters selected at $z\sim2.23$ in the CALYMHA survey, which stand at a mean of 0.18. For the CIII] and CII] source with disky morphology as discussed in the previous section, the blue UV colours indicate a relatively dust-free environment.

For comparison, we also present a rest-frame $(U-B)_{\rm rest}$ colour, derived from the observed $i-z$ colour (Fig. 5). Our CIII] emitters are on average slightly bluer ($(U-B)_{\rm rest}=0.38$) than the spectroscopic sample of CIII] emitters at $z\sim1$ from Du et al. (2016), which characterise their emitters as being blue and low-mass with little dust extinction. Note however that the two distributions are perfectly compatible within the full distribution of values.

4.3 UV slope β

The dust in a galaxy absorbs the UV radiation coming from an AGN or from massive, young stars. Despite it depending on many other properties (see for example Bouwens et al. 2009), the slope of the rest-frame UV continuum (β) is usually used as a simple tracer of the dust extinction in a galaxy. Here, we estimate β for our CII], CIII] and CIV emitters, defined in the following way:

$$\beta=-\frac{m_1-m_2}{2.5\log_{10}\left(\frac{\lambda_1}{\lambda_2}\right)}-2, \quad (2)$$

where m_1 and m_2 are the magnitudes of the source in two observed filters which trace the rest-frame UV, preferentially around the 1500 Å reference wavelength. λ_1 and λ_2 are the central wavelengths of the two filters.

Given that our emitters are at 3 different redshifts, it is not simple to have filters that trace exactly the same rest-frame wavelengths. The best choices of filters to trace the rest-frame UV included the *U* filter, which can be contaminated by the emission lines. We chose filters to match the convention used in other studies and ease comparisons:

- CII]: NUV, U
- CIII]: U, B
- CIV: U, V

Note that for CIII] emitters, the *U* filter traces a slightly redder rest-frame wavelength compared to other studies and CII] and CIV, which may bias β to slightly redder values.

We list the averages of the β slope in Table 3. The β slopes of our emitters indicate a steep UV continuum with potential low dust attenuation, within the same ranges as Lyα emitters at $z\sim2.23$, but with CIII] being slightly redder.

We show the average β slope compared to the average absolute UV magnitude $M_{\rm UV}$ in Fig. 6. The relation between the UV slope and absolute UV magnitude has been shown to not depend significantly on redshift for LBGs, thus making it a good probe for studying galaxies at all cosmic epochs (Bouwens et al. 2009; Smit et al. 2012).

Fig. 6 shows that the CII] and and CIV emitters are consistent in UV properties with other Lyman break selected SF galaxies at higher redshift ($z\sim2.5-4$, Bouwens et al. 2009) and with Lyα se-

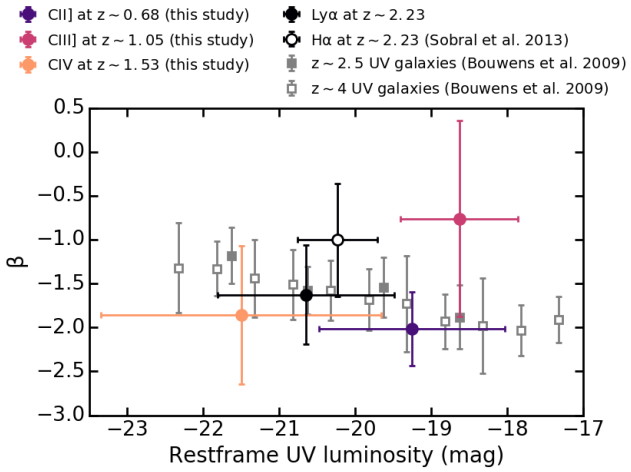

Figure 6. Distribution of rest-frame UV slope β as function of UV magnitude for our sample of emitters and Lyα (Sobral et al. 2017) and Hα at $z \sim 2.23$ (Sobral et al. 2013). Only sources with both rest-frame UV bands detected are plotted. For comparison, we plot the values for $z \sim 2.5$ and $z \sim 4$ Lyman break, UV selected galaxies from Bouwens et al. (2009). CII] and CIV emitters have colours consistent with the population of UV selected galaxies. CIII] emitters are redder, consistent with more general populations of SF galaxies such as those selected through Hα.

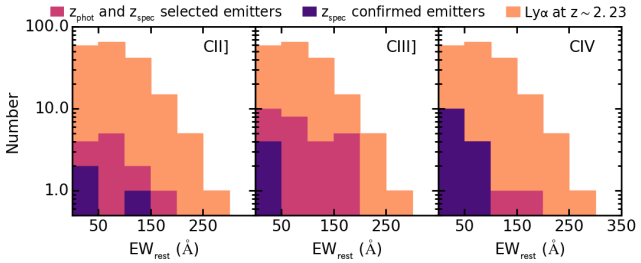

Figure 7. Rest-frame EW distribution for highly secure CII], CIII], CIV, classified as such by spectroscopic or photometric redshifts. We removed any potential high redshift sources which were classified as C species based on $z_{\rm phot}$, but as $z > 2$ sources by colour-colour selections from Sobral et al. (2017) or by Lyman break colour cuts. Note the large average EW for all three emitter types. For comparison, we also show the EW distribution of the Lyα emitters at $z \sim 2.23$ selected in Sobral et al. (2017).

lected galaxies at $z \sim 2.2$. It is important to note that Lyα and LBG selected samples are generally biased towards blue, less massive, metal-poor SF galaxies (Oteo et al. 2015). Note that Lyα can also probe extremely dusty galaxies unlike the LBG technique (Oteo et al. 2015; Matthee et al. 2016). The average β slope is consistent with the results obtained from the observed and intrinsic colours, indicating that CII] and CIV emitters are relatively blue objects with little dust extinction. At first glance, this is quite surprising, because, as was discussed in previous sections, a large fraction of CII] emitters and the bulk of CIV emitters have properties consistent with AGN. However, young, dust-free, quasar-like AGN will have steep UV continua, similar to those measured for CIV and CII] emitters.

CIII] emitters have relatively flat slopes, indicating a redder UV continuum. This means CIII] emitters have β slopes consistent with more general populations of SF galaxies such as those selected from Hα (Oteo et al. 2015). The CIII] emission line may therefore be a good, unbiased tracer of SF galaxies with a range of properties.

4.4 EW$_{\rm rest}$ distribution

We also investigate the distribution of rest-frame $EW_{\rm rest}$ in the sample of emitters. We find that the average EWs are high. This could be caused by Lyα interlopers, which can have large observed EWs.

Therefore, as a further conservative step, we attempt to bring any contamination from Lyα emitters (which may have high EWs) to virtually zero. We do this by applying colour cuts targeting the Lyman break in $z \gtrsim 2$ galaxies to further remove any potential Lyα interlopers from the sample:

$$(NUV - U) > 1.0 \quad \text{or} \quad (NUV - B) > 1.5 \qquad (3)$$

The distributions of the resulting samples with very high purity are given in Fig. 7. Averages are listed in Table 3, while individual values are given in Tables B1, B2 and B3. We find a significant population with large rest-frame EWs for all three emitter species, potentially extending up to 200 Å. A word of warning is that the errors on the rest-frame EW can be large, with an average of ~ 60 per cent of the EW value. Hence, some of the values can be 60 per cent lower or higher than estimated here. Furthermore, as we will discuss in Section 4.5, our morphological results show that we may be tracing specific regions within galaxies with little to no UV continuum, which may bias the EW towards higher values.

Spectroscopic observations are necessary to pose tighter constraints on the EW values, reduce the error bars and further investigate the validity of NB observations for measuring the EW of CII], CIII] and CIV emitters. EW could also be overestimated due to variable sources, which we discuss in detail in Section A. While variability could explain part of the population, the entire population of large EW sources cannot be explain this way.

Another possibility to explain the large EW are offsets between the main line emission region and the galaxy stellar light. Such offsets could be caused by systematic astrometric errors, but can also be caused by a real physical separation in the peaks of the underlying continuum and the line emission. While investigating this avenue with the INT NB data alone is not possible because of the large point spread function (psf, ~ 2 arcsec), we discuss this in more detail using high resolution *HST* data in Section 4.5. As will be shown in Section 4.5, astrometric errors are likely not the cause of the large EW.

The distribution of rest-frame EW for the CII] emitters extends up to 200 Å (as shown in Fig. 7). The chances of all of these high EW sources being interlopers or variable sources is small as explained above. We have also been extremely conservative in our selection and one source with a large $EW_{\rm rest}$ of 84 Å as measured from our NB data has a spectroscopic redshift confirming it to be a CII] emitter at $z \sim 0.68$ (although this specific source could still be variable).

The rest-frame EW distribution of CIII] emitters extends up to large values, with an average of ~ 100 Å (Fig. 7). These values place our CIII] sample in a different regime than other samples from the literature. Very recently, Du et al. (2016) published a spectroscopically-selected CIII] sample at $z \sim 1$ with a median $EW_{\rm rest}$ of 1.3 Å. They also compared with results from the literature at redshifts up to ~ 6 and found that, on average, the CIII] emitters discovered till now have EW of at most ~ 25 Å and are hosted by young, low mass, SF galaxies. The average EW of our CIII] emitters is also higher than what was found by Shapley et al. (2003) in stacks of LBGs, where their strongest Lyα emitters have mean rest-frame CIII] EW of about 10 per cent of Lyα, or ~ 5.4 Å. Note

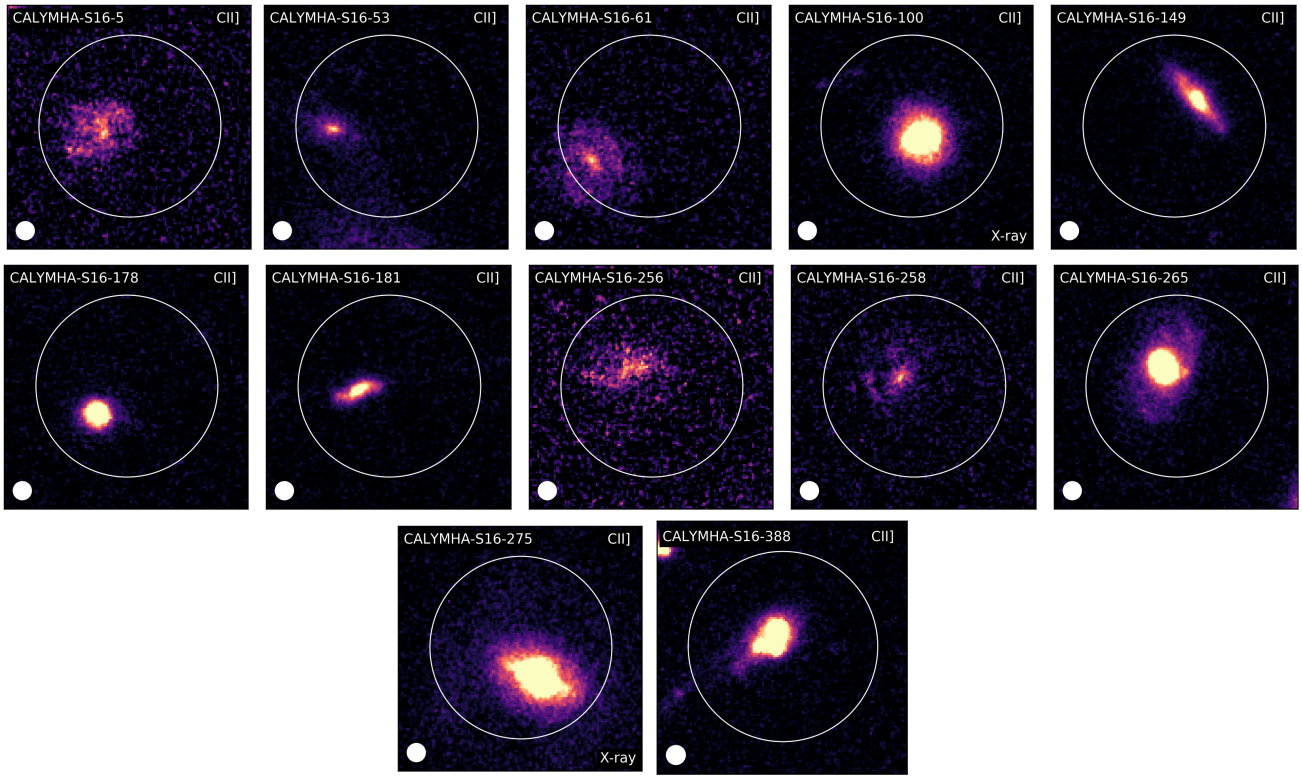

Figure 8. *HST* cutouts of $z \sim 0.7$ CII] emitters selected based on $z_{\rm spec}$ or $z_{\rm phot}$. Images are on the same colour scale, from 0 to $20 \times \sigma_{\rm RMS}$, with a size of $4'' \times 4''$. At the redshift of CII] emitters, the images have a size of 28.3 kpc on each side. The large circle represents the $3''$ aperture used to extract photometry for the CALYMHA sources. The small circle represents 3 times the *HST* point-spread function (PSF $\sim 1''$), encompassing 98 per cent of the flux. We also indicate whether the source has an X-ray or radio counterpart. Note that some sources simply do not have X-ray or radio counterparts, while others are not covered with such data. While some CII] emitters have disky morphologies, some have very bright nuclei, which in the case of source 275 correlates with an X-ray detection, indicating these galaxies are Seyfert-like. We center the *HST* thumbnails on the peak position of the emission line and find that, in some cases, there are offsets of ~ 5 kpc from the peak UV rest-frame emission. This may explain the relatively large EW we measure.

however that all these sources are continuum selected, which will bias samples towards low EWs, while our samples are line emission selected, thus finding higher EWs. As mentioned earlier, any offset between the line emitting region and the stellar light could also explain the large EW we are measuring. Therefore, for continuum selected sources, placing the spectroscopic slit or fibre on the main continuum emitting region does not guarantee the line emission will be captured. Spectroscopy focusing on the line-emitting regions is however crucial to unveil the nature of these emitters and understand the source of the high EW emission.

The CIV emitters have average rest-frame EWs of 52 Å. It is important to note that a significant fraction of these are also spectroscopically confirmed, including a source with a EW of ~ 100 Å measured using the NB and BB data (see Fig. 7). The values are consistent within the ranges measured from a large sample of ~ 150 Type II quasars at $z \sim 2-4.3$ by Alexandroff et al. (2013). They measure rest-frame EW ranging from 10 to 100 Å for their most secure Type II sample, with an average of about 40 Å. Note that the average CIV line fluxes in Alexandroff et al. (2013) are about $(1-1.2) \times 10^{-16}$ erg s^{-1}, which is smaller than our average of 7.7×10^{-16} erg s^{-1}, but consistent within the spread of the values. Without spectroscopic information, many of our CIV sources would have been likely Lyα candidates at higher redshifts. While traditionally it has been assumed that large EW emitters are Lyα, without clear, secure redshift information the emitter can be misidentified. It thus becomes apparent that CIV emitters can represent an important contaminating population, as was concluded in Sobral et al. (2017) and in Stroe et al. (2017b).

4.5 *HST* morphologies

Ancillary high-resolution space based optical data is crucial in unveiling the nature of our emitters, especially in understanding their colour properties from Sections 4.1, 4.2 and 4.3 and their high EWs (Section 4.4). For the sources with coverage in *HST*, we show their morphologies in Figs. 8, 9 and 10. The optical properties of the emitters are listed in Tables B1, B2 and B3 .

Twelve out of the 16 CII] sources have *HST* coverage, revealing a mix of morphology types. Seven CII] emitters have a disky or spiral morphology, while four have a very bright nucleus and a spiral structure, indicative of a Seyfert nature. These Seyfert-like sources are also the most luminous in the emission line and have the lower EW (see Section 4.4). The possible mixed nature of CII] emitters, some being powered by SF and some by AGN is therefore not only supported by the optical and UV colours of the emitters (Sections 4.1, 4.2, 4.3), but also by the morphologies.

Out of our 24 CIII] sources, there are 19 with *HST* coverage, presenting a wide variety of morphologies. Some CIII] emitters have a spiral structure, others a disturbed morphology and multiple nuclei, others consisting of 2 or more interacting components. There are also two sources with a UV bright core, indicative of

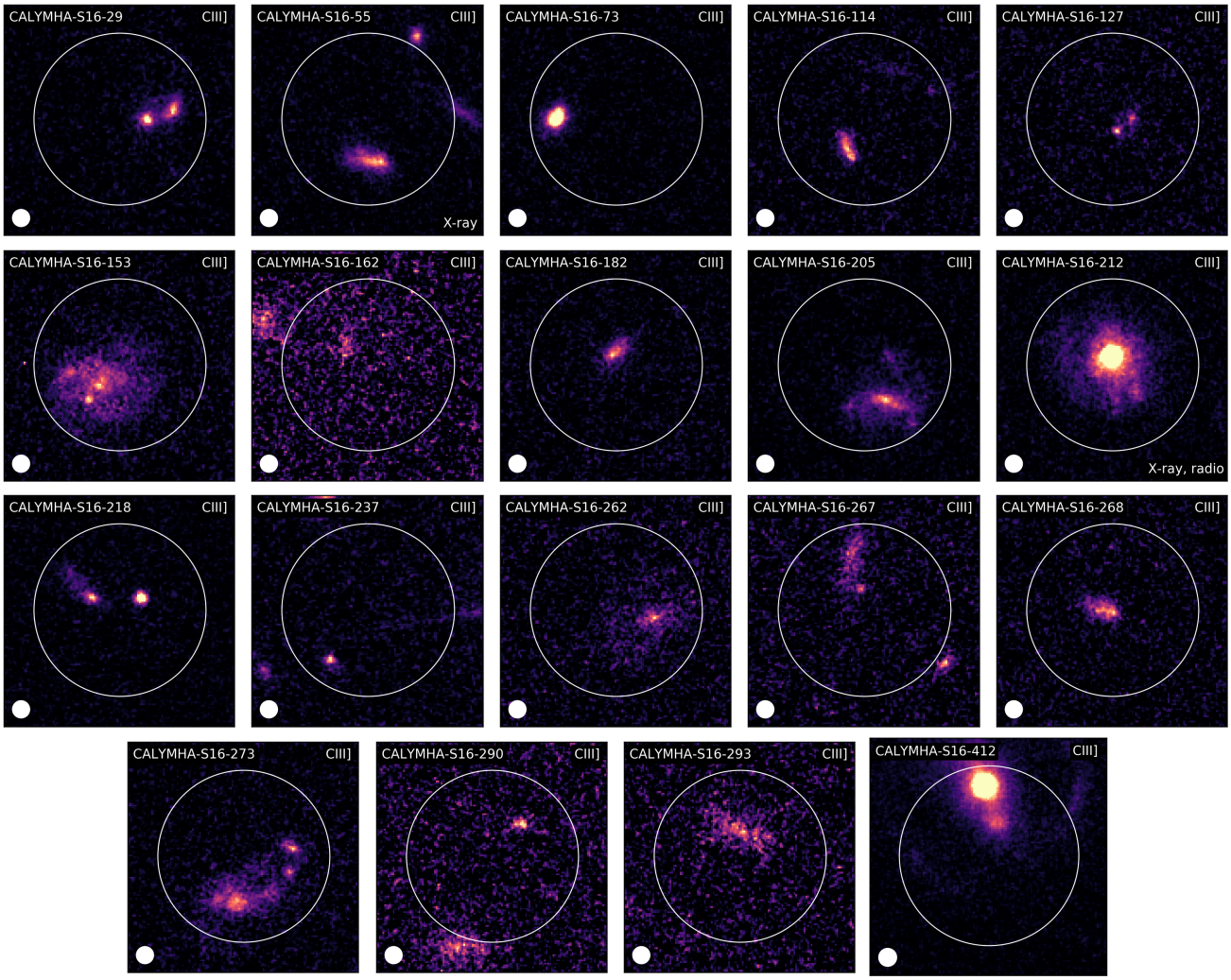

Figure 9. Same as Fig. 8, but for CIII] emitters. The images are 32.4 kpc in size at the redshift $z \sim 1.05$ of the CIII] emitters. The large circle is the 3″ aperture used to extract photometry, while the small circle is 3×PSF of *HST* point-spread function, which captures 98 per cent of the flux for a point source. CIII] emitters have a range of optical morphologies, including disks, many interacting or merging sources and messy, complicated, disturbed galaxies. Source 212 has a Seyfert-like morphology with a bright optical core and a radio and X-ray counterpart. Note that in many cases the rest-frame continuum is offset from the CALYMHA emission line detection, which may explain the large *EW* we find. This is likely caused by physical offsets between the stellar continuum and the brightest emission line regions. A small fraction of sources with coverage have either X-ray or radio detections, indicative of an AGN.

a Seyfert nature, which are also among the brightest in the CIII] emission line.

Ten out of 17 CIV sources have space telescope coverage and they are all point sources even at *HST* resolution. The *HST* data support a scenario where CIV emitters are predominantly quasars: all four sources with *Chandra* coverage have a direct X-ray detection, with an additional three sources with a radio detection. We note that the line luminosities of these sources span the $L_{\rm CIV} \sim 10^{42.6} - 10^{42.9}$ erg s^{-1} range.

We find that many line emitters, especially CII] and CIII] are offset from the *HST* detection. Note that the offsets are more prevalent for disky galaxies, e.g. for CIII] emitters, while no large offsets are detected in the CIV emitter sample. It is important to note that sources where the galaxy disk is most offset from the emission line detection in CALYMHA are also among the sources with the largest EW (see discussion of the large EW in Section 4.4). A reason for large $EW_{\rm rest}$ could be the offset between the main line emission region and the location of the bulk stellar light. Therefore, we have tentative evidence that some of the emission line regions can be offset by 1″ from the brightest UV continuum component, which would result in large *EW* (see Figs. 8 and 10). While the offset can be caused by a physical displacement, a caveat to note is the large PSF of the NB and BB INT observations used to calculate the EW, which can be prone to larger astrometric uncertainties and thus contribute towards the offsets we are measuring. We investigate the offset between CALYMHA sources and the *HST* counterparts and found that astrometric errors are in the $0.2 - 0.3$ arcsec range, which is the expected value for INT observations (Sobral et al. 2017). Therefore, the large offsets found here are most likely of a physical origin, either by the presence of an AGN, and in the case of SF sources, by an offset between the stellar light and the line emitting region. Another option, at least for some of the sources which are not spectroscopically confirmed, would be that they are in fact higher redshift, lensed Lyα emitters. This may explain the offsets as well as the large EW.

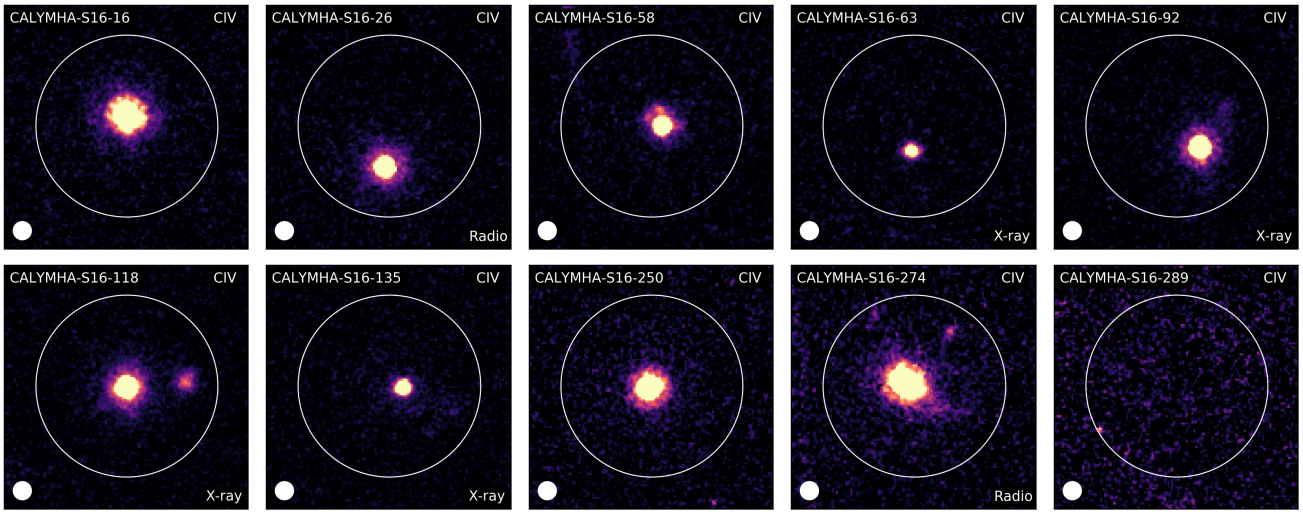

Figure 10. Same as Fig. 8, but for CIV emitters. The cutouts trace 33.9 kpc on each side, at the redshift of CIV ($z \sim 1.53$). The large circle represents the 3″ CALYMHA aperture is marked with the large circle and the small circle is 3 times the *HST* PSF. All the sources are consistent with being point-sources, with their flux contained within the PSF of *HST*. Six out of ten sources with *HST* coverage have either radio or X-ray counterpart, further supporting a scenario where CIV sources are power almost exclusively by AGN. Note that all sources with X-ray coverage do have a counterpart. Unlike, CII] or CIII] emitters, the CIV line detections are well centred with respect to the *HST* and thus more consistent with astrometric errors rather than physical offsets. An AGN powering source for CIV can readily explain the large EW.

4.6 *Chandra* X-ray and VLA radio counterparts

While no emitters have direct FIR detections (and thus none can be extremely star-forming at the 1000 $M_\odot\,yr^{-1}$ level), some sources do have an X-ray or radio counterpart, which we discuss here and summarise in Table 4. Five CII] have *Chandra* coverage and 13 are covered by radio data. Nine CIII] sources are covered with *Chandra* and 22 with radio coverage, while 4 CIV are covered with X-ray and 13 with radio.

In the case of CII], the results from the optical morphologies and colours are supported by the X-ray data: the disk galaxies with *Chandra* coverage do not have an X-ray counterpart, while the Seyferts have counterparts. None of the CII] sources is active in the radio (out of 13 with coverage). The *HST* data reveals that some of the CII] emitters have a spiral-like morphology. In that canse any radio emission will be powered by SF, which is low compared to AGN-powered radio emission. Additionally, only 5 per cent of Seyferts are radio-loud. Therefore, the lack of radio detection for CII] emitters is not surprising given the depth of the radio observations.

As mentioned in Section 4.5, the CIII] sources have a range of morphologies. One of the two sources with a UV bright core, indicative of a Seyfert nature, has coverage in *Chandra* and VLA and possesses an X-ray and radio detection. As expected for normal SF galaxies, none of the other CIII] sources have radio or X-ray counterparts. A detection would imply very large SFRs of $\sim 1000\,M_\odot\,yr^{-1}$.

The radio and *Chandra* data for CIV, in agreement with *HST*, support a scenario where CIV emitters are predominantly quasars: all four sources with *Chandra* coverage have a direct X-ray detection, with an additional three sources with a radio detection.

In conclusion, the X-ray and radio data suggest that CIII] is mostly powered by SF. CIV and some CII] emitters are active in the X-ray, indicating they are young, actively accreting in the radiatively driven, quasar mode. Only a few CIV and no CII] have radio detections, which would be indicative of a more evolved AGN in the mechanical, radio-loud phase.

4.7 Average SFRs and BHARs

4.7.1 *Chandra stacking*

To evaluate the level of activity of the central supermassive black hole in our emitters, we can estimate the black hole accretion rate (BHAR) which can be derived from X-ray data. We follow the method described in Calhau et al. (2017) to measure the average BHAR for the CII], CIII] and CIV emitters by stacking sources with *Chandra* coverage.

We make a $20'' \times 20''$ cutout around the position of each source and take the mean to obtain an average image which is used to calculate the average flux of the emitters. We establish a stacking radius of 2 arcsec and convert the counts inside to flux by following the indicated procedure in Elvis et al. (2009), with a photon index Γ of 1.4 and Galactic absorption of 2.7×10^{20} cm^{-2}. We convert the flux F_X to an X-ray luminosity L_X using:

$$L_X = 4\pi D_L^2 F_X (1+z)^{\Gamma-2} \quad (erg\,s^{-1}), \tag{4}$$

We obtain the bolometric luminosity by multiplying by 22.4 (Lehmer et al. 2013). The BHAR is obtained by:

$$BHAR = \frac{(1-\varepsilon)L_{bol}}{\varepsilon c^2} \quad (M_\odot\,yr^{-1}), \tag{5}$$

where $\varepsilon = 0.1$ is the accretion efficiency (following Lehmer et al. 2013) and c is the speed of light. Errors on both L_X and the BHAR are calculated by taking the standard deviation of the distribution obtained from a bootstrapping analysis of the data.

4.7.2 *FIR and radio stacking*

We use FIR and radio data to obtain an average SFR in our sources.

To obtain an estimation of the dust-obscured SFR from the

Table 4. Summary of the optical, X-ray and radio properties of CII], CIII] and CIV emitters. The full details on individual sources can be found in Tables B1, B2 and B3.

Line	*HST*		*Chandra*		Radio 1.4 GHz	
	coverage	morphology	coverage	counterpart	coverage	counterpart
CII]	12/16	4 bright-core+disk, 7 disky, 1 interacting	5/16	2/5	13/16	0/13
CIII]	19/34	2 bright-core+disk, 8 disturbed/interacting, 7 diffuse/spiral, 2 compact	9/34	1/9	22/34	1/22
CIV	10/17	10 point sources	4/17	4/4	12/17	3/14

FIR emission, we start by mean stacking our sources using the *Herschel* bands at 100, 160, 250, 350 and 500 μm (PACS and SPIRE instruments). Aperture corrections were applied for the PACS 100 and 160 μm bands as specified in the PACS PEP release notes. In the SPIRE 250, 350, 500 μm, the fluxes were taken from the peak value in each stack. Note that we do not have any detections and can only provide upper limits. We estimate the FIR luminosities by fitting modified black body templates (using the SWIRE template Library, Polletta et al. 2007) to the upper limits and integrating the best fit between 8 and 1000 μm. We use the total FIR luminosity $L_{\rm FIR}$ to compute the SFRs, assuming a Chabrier (2003) IMF by using:

$$SFR_{\rm FIR} = 2.5 \times 10^{-44} L_{\rm FIR} \quad {\rm M}_\odot\,{\rm yr}^{-1}. \qquad (6)$$

We find no detections in any of the stacks and thus can place upper limits on the SFRs. The results of the stacking do not change if we use all sources with coverage or only the sources with *Chandra* coverage.

Radio at 1.4 GHz can be used as a dust-free SF indicator on timescales longer than FIR or emission lines. The radio stacking procedure is the same as the X-rays. To convert the radio luminosities $L_{\rm radio}$ to SFRs, we use the conversion determined by Yun et al. (2001), adapted to a Chabrier (2003) IMF:

$$SFR_{\rm radio} = 3.18 \times 10^{-22} L_{\rm radio} \quad {\rm M}_\odot\,{\rm yr}^{-1}. \qquad (7)$$

Note that in the case of radio, unlike FIR, a direct detection is caused by an AGN rather than SF. We find that if we remove all detections, our radio stacks all provide non-detections in the same range as the FIR ones.

4.7.3 *Stacking results*

The results of our X-ray, FIR and radio stacking analysis are listed in Table 5. The stacked X-ray image can be found in Fig. 11, which shows clear detections for CII] and CIV and a very faint/non detection for CIII]. We plot our *BHAR* results and compare with similar measurements obtained for Hα and FIR selected SF galaxies, Lyα emitters and AGN (Delvecchio et al. 2015; Stanley et al. 2015; Calhau et al. 2017, Calhau et al. in prep) in Fig. 12. Note however the low number statistics, driven by the small area of the publicly available *Chandra* images.

The stacking analysis indicates that CII] emitters are bright in the X-rays and are consistent with AGN activity ($BHAR = 0.10 \pm 0.06\ M_\odot\ {\rm yr}^{-1}$), as revealed by Fig. 12. CII] emitters accrete matter onto their BH at a much higher rate than SF galaxies. The CII] emission, as suggested, for example, by Best et al. (2002) could then be in part powered by shocks near the BH.

Once the only source with an X-ray detection is removed, CIII] emitters have an upper limit X-ray luminosity consistent with SF activity and a low BHAR ($0.02 \pm 0.01\ M_\odot\ {\rm yr}^{-1}$), similar to what

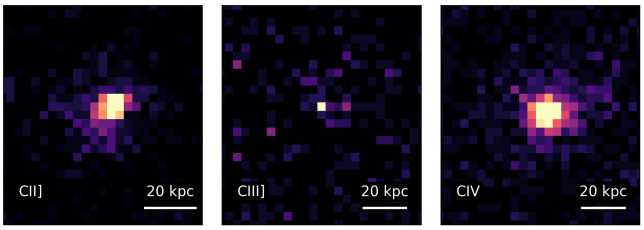

Figure 11. The X-ray stack for sources with coverage in COSMOS with *Chandra*. The CII] and CIV detections are consistent with AGN activity with large X-ray luminosities of $10^{43.5}$ and $10^{44.4}$ erg s^{-1}, respectively. The much fainter CIII], with an average X-ray luminosity of $10^{42.8}$ erg s^{-1}, is likely dominated by SF galaxies with a very minor AGN contamination, consistent with our results. The images are on the same colour scale.

is measured from Hα and FIR selected SF galaxies (Delvecchio et al. 2015; Calhau et al. 2017).

The average X-ray luminosity of the CIV sources is very high, $\sim 10^{44.4}$ erg s^{-1}, supporting an active nucleus which accretes matter at a rate of $\sim 0.83\ M_\odot\ {\rm yr}^{-1}$. This value is well above the rate expected for main sequence SF galaxies, lying in the AGN region of Fig. 12. This is consistent with the optical properties of the CIV emitters discussed in previous sections.

There are no detections in the FIR bands, so we are only able to provide 3σ SFR upper limits of 15, 75, 141 M$_\odot$ yr^{-1} for CII], CIII], CIV, respectively. Note that the different values are mostly driven by the different redshifts of the three types of emitters. The FIR non-detections are mostly caused by the relatively low number of sources in each stack compared to the detections from Calhau et al. (2017), who stacked about ten times more sources than included in this analysis. In order to further test this, we stack the Hα emitters at $z \sim 0.84$ in the FIR, using the same number of sources as our CIII] emitters and find no detection. We therefore conclude that CIII] emitters are fully consistent with being similar to Hα selected samples at a similar redshift, including the fact that, as seen before, they are slightly redder than LBGs.

Similarly, we do not have a detection in the radio stacks after removing direct detections (which are caused by AGN, not SF). These upper limits, as for the FIR, are not very stringent ($\sim 17, 35, 115\ M_\odot\ {\rm yr}^{-1}$ for CII], CIII] and CIV respectively). The range of typical SFR from Hα emission at $z \sim 0.8-1.5$ is in the range $8-16\ M_\odot\ {\rm yr}^{-1}$ (Sobral et al. 2013), well below our FIR and radio depths.

5 DISCUSSION

We investigate the nature of CII], CIII] and CIV line emitters by jointly interpreting their emission line properties with broad band optical colours as well as ancillary space-based optical and X-ray data.

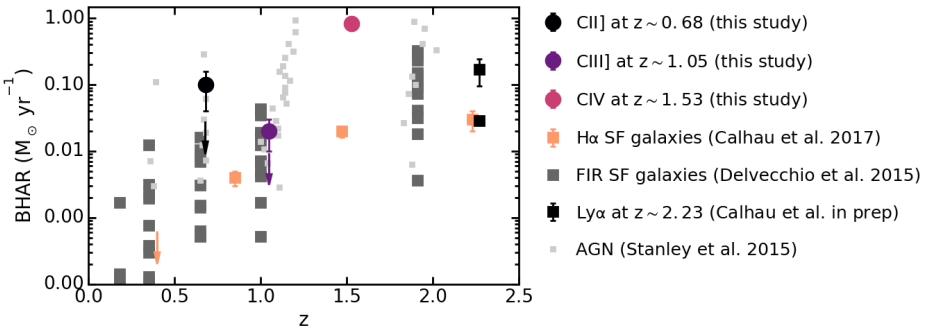

Figure 12. The black hole accretion rate (*BHAR*) for the stacked CII], CIII] and CIV sources, obtained by converting their average X-ray luminosities into accretion rates. All CIV sources are directly detected in the X-ray. Upper limits for CII] and CIII] stacks are given with direct detections removed. CII] emitters have a high average *BHAR*, similar to AGN. CIII] emitters have *BHAR* similar to Hα selected, main sequence SF galaxies. CIV emitters have extremely high accretion rates, consistent with bright quasars. We also plot the *BHAR* for Hα selected, SF galaxies (Calhau et al. 2017). Overplotted in dark grey are main-sequence, FIR selected SF galaxies from Delvecchio et al. (2015). The different values are stacks for galaxies of different masses and SFRs. The light grey points represent AGN from Stanley et al. (2015) stacked in different luminosity bins. We also plot the result for Lyα emitters at $z \sim 2.23$ from Calhau et al. (in prep), with and without the direct X-ray detections included in the stacks.

Table 5. Average X-ray luminosity and BHAR, as resulting from a stacking analysis of the CII], CIII] and CIV emitters (with $z_{\rm spec}$ or $z_{\rm phot}$), including direct detections. While CII] and CIV emitters are consistent with AGN activity, CIII] values place in the SF galaxy regime. Note that removing the direct X-ray detections results in non-detections in the stacks because of the very low numbers of sources left. We also present SFR upper limits obtained from FIR and radio data. Note that individual detections are removed from the radio stack as a direct radio detection will be caused by an AGN rather than SF (which is the purpose of our radio stacks).

Line	$\log L_{\rm X}$ (erg s^{-1})	*BHAR* ($M_\odot$ yr^{-1})	No sources	$SFR_{\rm FIR}$ 3σ upper limit ($M_\odot$ yr^{-1})	$SFR_{\rm radio}$ 3σ upper limit ($M_\odot$ yr^{-1})
CII]	43.46 ± 0.56	0.10 ± 0.06	5	< 15	< 17
CIII]	42.80 ± 0.37	0.02 ± 0.01	9	< 75	< 35
CIV	44.37 ± 0.08	0.83 ± 0.12	4	< 141	< 115

5.1 CII] emitters $z \sim 0.68$

CII] emitters at $z \sim 0.68$ have optical colours spanning across the colour space of SF galaxies at their redshift into a regime more typical of SF sources at higher cosmic distances. Such unusual optical colours may indicate that while part of the CII] emitter population is powered by SF, at least some sources host an AGN, in agreement with luminosity function and cosmic ratio results from Stroe et al. (2017b). This is also supported by the *HST* morphology of CII] sources: while some sources have spiral-like morphologies, part of the population, particularly the sources with atypical colours, have a bright nucleus accompanied by a disk. While the bright nucleus could be indicative of a nuclear starburst surrounded by a stellar disk, this scenario is not supported by the X-ray data which reveals that these CII] emitters have BHAR rates consistent with an AGN at their core. CII] emitters have relatively steep β slopes, which indicate a relatively blue UV continuum. This is also supported by the lack of a detection in the FIR stacks of these sources. CII] emitters also have high rest-frame EWs, which could be caused by either the offset we observe between the main stellar disk and the line emitting region, or by AGN activity.

Traditionally, it was thought that CII] emission is mostly triggered in shocks around AGN (De Breuck et al. 2000; Best et al. 2000, 2002), however this resulted from studies of this line being done almost exclusively in bright, active galaxies. Overall, our results indicate that CII] emitters may actually powered in part by blue, SF galaxies at lower luminosities and in part by Seyfert-like sources with young, actively-accreting AGN at brighter line luminosities.

5.2 CIII] emitters at $z \sim 1.05$

Most CIII] emitters at $z \sim 1.05$ have optical colours consistent with SF galaxies at their redshift. Furthermore, their low average BHAR is also consistent with SF galaxies. The β UV slopes of CIII] emitters are consistent with Hα selected galaxies, indicating CIII] emission might be suitable avenue for selecting a wide range of SF galaxies. CIII] sources are also mostly X-ray and radio quiet, as expected for SF galaxies. Most emitters have disky, clumpy or disturbed optical morphologies, indicative of either single or interacting SF galaxies. The offset optical disk or the clumpy/disturbed morphologies might explain the large EW we find for some CIII] emitters. The few direct X-ray and radio detections (< 10 per cent) correlate with a bright nucleus plus a disk optical morphology, which indicates that the brightest CIII] emitters host an AGN at their core.

Traditionally CIII] emission was thought to originate from AGN. More recent results focusing on SF galaxies find that ~ 20 per cent of local galaxies have the CIII] feature and the strongest CIII] emission is fostered at low metallicities (Rigby et al. 2015). Part of their sample are Wolf-Rayet galaxies, indicating recent (few Myrs), short-lived (< 1 Myr) strong starbursts. At higher redshifts ($1.5 - 3$), Stark et al. (2014) find that almost all of their CIII] emitters also possess strong Lyα. Stanway et al. (2016), in agreement with Jaskot & Ravindranath (2016), showed that the presence of binary stars can increase the ionising flux by up to 60 per cent in low metallicity ($< 0.3 Z_\odot$) environments, which could also lead to a boost in CIII] production.

While these works indicate that strong CIII] is produced in

relatively low-metallicity SF galaxies, our results strongly support a scenario where CIII] emitters trace a more general population of SF galaxies at $z \sim 1$, with very few bright emitters being powered by AGN. This is similar to what is found in studies of Lyα and Hα emitters at $z > 2$ (Matthee et al. 2015; Konno et al. 2016; Sobral et al. 2017; Matthee et al. 2017). However, as shown in Stroe et al. (2017b), at fixed UV magnitude of line flux, the number density of CIII] emitters is substantially lower than Hα or LBG SF galaxy populations, indicating only a fraction of galaxies have strong CIII]. The average line ratios imply that CIII] is ~ 20 times fainter than Hα and ~ 4 times fainter than observed Lyα (Stroe et al. 2017b).

5.3 CIV emitters $z \sim 1.53$

The direct detections in the X-ray, the high accretion rates characteristic for bright AGN, the universal optical quasar morphologies, the unusual optical colours and blue UV slopes and large rest-frame EW, all reveal that CIV is produced in intense radiation fields characteristic to young, virtually dust-free actively accreting quasars. The number distribution of CIV emitters as function of line luminosity also indicates they are primarily a quasar population, being well described by a power-law (Stroe et al. 2017b).

In a sample of lensed, low mass galaxies at $z \sim 1.5 - 3$, Stark et al. (2015a) find ubiquitous joint detections of CIV and CIII], which require young stellar populations, increased electron temperatures and an enhanced ionising output from metal poor gas and stars. Their work therefore indicates that part of the CIV emission is driven by strong AGN activity, while some is powered by young stars.

Our results however, seem to support a scenario where the bulk of the CIV is produced in galaxies hosting powerful AGN at least at $z \sim 1.5$. One important aspect to note is that the rest-frame UV magnitudes of the sources from Stark et al. (2014) are similar to ours, so a comparison is appropriate, although the redshift is different.

6 CONCLUSIONS

We characterise the properties CII], CIII] and CIV emitters at $z \sim 0.68, 1.05, 1.53$. These sources were selected from the first blind, statistical study of Carbon emitters, uniformly selected in the COSMOS and UDS field as part of the CALYMHA survey. In this paper, we focus on the UV, optical, X-ray, FIR and radio properties of these emitters. Our main results are:

- CII] emitters at $z \sim 0.68$ have disky structure or bright nucleus with a disk morphology (Fig. 8) and blue UV colours (Figs. 4, 6). Some of the brightest line emitters are strong X-ray sources (Fig. 11), with black hole accretion rates (Fig. 12) characteristic of AGN. Our results therefore indicate that CII] traces a mixed population of SF galaxies and AGN, especially at the brightest line luminosities. For the brighter emitters, our results are in accordance with the theoretical expectation that CII] emission is triggered by shocks around AGN.
- CIII] emitters at $z \sim 1.05$ in our study have typical optical colours for SF galaxies (Fig. 3) and morphologies indicative of either isolated or interacting galaxies (Fig. 9). Their relatively blue rest-frame UV and optical colours (Figs. 5, 6) and low black hole accretion rates (Fig. 12) are consistent with general populations of SF galaxies.
- The point-like *HST* morphologies (Fig. 10), the strong X-ray detections implying high accretion rates (Figs. 11, 12) and the blue optical and UV colours (Figs. 4, 6) indicate that CIV emitters are almost universally blue/non-dusty quasars.
- We discover a large, previously-undetected population of CII], CIII] and CIV emitters with large rest-frame EW, of above 50 Å, potentially up to 200 Å (Fig. 7). In stark contrast, the typical EW of continuum selected CIII] samples from the local Universe up to $z \sim 6$ is $\lesssim 25$ Å. These large EW might be caused by emission line regions offset from the stellar disk or because of the AGN nature of some of the sources.

While historically thought to originate in AGN, our study revealed some interesting properties of CII], CIII] and CIV emitters at $z \sim 0.7 - 1.5$. While CIV emitters are almost universally quasars, CIII] emission is consistent with being produced in a wide variety of SF galaxies and CII] emission may trace either an AGN or SF. Further spectroscopy is crucial however to unveil their powering source and the physics of the large EW we measure in a fraction of the population. In the companion paper, Stroe et al. (2017b), we further explore the samples and derive luminosity functions and cosmic average line ratios.

ACKNOWLEDGEMENTS

DS acknowledges financial support from the Netherlands Organisation for Scientific research (NWO), through a Veni fellowship. CALYMHA data is based on observations made with the Isaac Newton Telescope (proposals 13AN002, I14AN002, 088-INT7/14A, I14BN006, 118-INT13/14B, I15AN008) operated on the island of La Palma by the Isaac Newton Group in the Spanish Observatorio del Roque de los Muchachos of the Instituto de Astrofísica de Canarias. Also based on data products from observations made with ESO Telescopes at the La Silla Paranal Observatory under ESO programme IDs 098.A-0819 and 179.A-2005. We are grateful to E. L. Wright and J. Schombert for their cosmology calculator. We would like to thank the authors of NumPy (van der Walt et al. 2011), SciPy (Jones et al. 2001), Matplotlib (Hunter 2007) and AstroPy (Astropy Collaboration et al. 2013) for making these packages publicly available. This research has made use of the NASA/IPAC Extragalactic Database (NED) which is operated by the Jet Propulsion Laboratory, California Institute of Technology, under contract with the National Aeronautics and Space Administration. This research has made use of NASA's Astrophysics Data System. This research has made use of the VizieR catalogue access tool, CDS, Strasbourg, France. The original description of the VizieR service was published in Ochsenbein et al. (2000). This research has made use of "Aladin sky atlas" developed at CDS, Strasbourg Observatory, France (Bonnarel et al. 2000; Boch & Fernique 2014). The CALYMHA catalogue used for this study is publicly available from Sobral et al. (2017).

REFERENCES

Alexandroff, R., Strauss, M. A., Greene, J. E., et al. 2013, MNRAS, 435, 3306
Allen, M. G., Dopita, M. A., & Tsvetanov, Z. I. 1998, ApJ, 493, 571
Astropy Collaboration, Robitaille, T. P., Tollerud, E. J., et al. 2013, A&A, 558, A33
Baldwin, J. A. 1977, MNRAS, 178, 67P
Bayliss, M. B., Rigby, J. R., Sharon, K., et al. 2014, ApJ, 790, 144
Bertin, E. 2006, Astronomical Data Analysis Software and Systems XV, 351, 112

Best, P. N., Röttgering, H. J. A., & Longair, M. S. 2000, MNRAS, 311, 23
Best, P. N., Inskip, K. J., Röttgering, H. J. A., & Longair, M. S. 2002, Revista Mexicana de Astronomia y Astrofisica Conference Series, 13, 155
Boch, T., & Fernique, P. 2014, Astronomical Data Analysis Software and Systems XXIII, 485, 277
Bonnarel, F., Fernique, P., Bienaymé, O., et al. 2000, A&AS, 143, 33
Bouwens, R. J., Illingworth, G. D., Franx, M., et al. 2009, ApJ, 705, 936
van Breukelen C., Cotter G., Rawlings S., et al. 2007, MNRAS, 382, 971
Calhau, J., Sobral, D., Stroe, A., et al. 2017, MNRAS, 464, 303
Capak, P., Aussel, H., Ajiki, M., et al. 2007, ApJS, 172, 99
Cirasuolo, M., McLure, R. J., Dunlop, J. S., et al. 2010, MNRAS, 401, 1166
Civano, F., Elvis, M., Brusa, M., et al. 2012, ApJS, 201, 30
Chabrier, G. 2003, PASP, 115, 763
Cowie, L. L., Barger, A. J., & Hu, E. M. 2010, ApJ, 711, 928
Dahle, H. 2006, ApJ, 653, 954
De Breuck, C., Röttgering, H., Miley, G., van Breugel, W., & Best, P. 2000, A&A, 362, 519
Delvecchio, I., Lutz, D., Berta, S., et al. 2015, MNRAS, 449, 373
Dijkstra, M. 2014, PASA, 31, e040
Ding, J., Cai, Z., Fan, X., et al. 2016, arXiv:1612.00902
Du, X., Shapley, A. E., Martin, C. L., & Coil, A. L. 2016, arXiv:1612.06866
Elvis, M., Civano, F., Vignali, C., et al. 2009, ApJS, 184, 158
Erb, D. K., Pettini, M., Shapley, A. E., et al. 2010, ApJ, 719, 1168
Favre, P., Courvoisier, T. J.-L., & Paltani, S. 2005, A&A, 443, 451
Feltre, A., Charlot, S., & Gutkin, J. 2016, MNRAS, 456, 3354
Geach J. E., Simpson C., Rawlings S., Read A. M., Watson M., 2008, VizieR Online Data Catalog, 838, 11369
Gutkin, J., Charlot, S., & Bruzual, G. 2016, MNRAS, 462, 1757
Hayes, M. 2015, PASA, 32, e027
Hunter, J. D. 2007, Computing In Science & Engineering, 9, 3, 90–95
Ilbert, O., Capak, P., Salvato, M., et al. 2009, ApJ, 690, 1236
Jaskot, A. E., & Ravindranath, S. 2016, ApJ, 833, 136
Jones, E., Oliphan, T., Peterson, P. et al. 2001
Kennicutt, R. C., Jr. 1998, ARA&A, 36, 189
Koekemoer, A. M., Aussel, H., Calzetti, D., et al. 2007, ApJS, 172, 196
Koekemoer, A. M., Faber, S. M., Ferguson, H. C., et al. 2011, ApJS, 197, 36
Konno, A., Ouchi, M., Nakajima, K., et al. 2016, ApJ, 823, 20
Laigle, C., McCracken, H. J., Ilbert, O., et al. 2016, ApJS, 224, 24
Lawrence, A., Warren, S. J., Almaini, O., et al. 2007, MNRAS, 379, 1599
Lehmer, B. D., Lucy, A. B., Alexander, D. M., et al. 2013, ApJ, 765, 87
Lilly S. J., Le Brun V., Maier C., et al. 2009, ApJS, 184, 218
Lowenthal, J. D., Koo, D. C., Guzmán, R., et al. 1997, ApJ, 481, 673
Mainali, R., Kollmeier, J. A., Stark, D. P., et al. 2016, arXiv:1611.071
Massey, R., Stoughton, C., Leauthaud, A., et al. 2010, MNRAS, 401, 371
Matthee, J., Sobral, D., Santos, S., et al. 2015, MNRAS, 451, 400
Matthee, J., Sobral, D., Oteo, I., et al. 2016, MNRAS, 458, 449
Matthee, J., Sobral, D., Best, P., et al. 2017, arXiv:1702.04721
Micheva, G., Iwata, I., & Inoue, A. K. 2017, MNRAS, 465, 302
Nilsson, K. K., Tapken, C., Møller, P., et al. 2009, A&A, 498, 13
Oliver, S. J., Bock, J., Altieri, B., et al. 2012, MNRAS, 424, 1614
Ochsenbein, F., Bauer, P., & Marcout, J. 2000, A&A, 143, 23
Ono Y., Ouchi M., Shimasaku K., et al. 2010, MNRAS, 402, 1580
Osterbrock, D. E., & Ferland, G. J. 2006, Astrophysics of gaseous nebulae and active galactic nuclei, 2nd. ed. by D.E. Osterbrock and G.J. Ferland. Sausalito, CA: University Science Books, 2006,
Oteo, I., Sobral, D., Ivison, R. J., et al. 2015, MNRAS, 452, 2018
Ouchi, M., Shimasaku, K., Akiyama, M., et al. 2008, ApJS, 176, 301-330
Polletta, M., Tajer, M., Maraschi, L., et al. 2007, ApJ, 663, 81
Rigby, J. R., Bayliss, M. B., Gladders, M. D., et al. 2015, ApJL, 814, L6
Sarajedini, V. L., Koo, D. C., Klesman, A. J., et al. 2011, ApJ, 731, 97
Schechter, P. 1976, ApJ, 203, 297
Schmidt, K. B., Huang, K.-H., Treu, T., et al. 2017, arXiv:1702.04731
Schinnerer, E., Carilli, C. L., Scoville, N. Z., et al. 2004, AJ, 128, 1974
Schinnerer, E., Sargent, M. T., Bondi, M., et al. 2010, ApJS, 188, 384
Shapley, A. E., Steidel, C. C., Pettini, M., & Adelberger, K. L. 2003, ApJ, 588, 65
Simpson C., Martínez-Sansigre A., Rawlings S., et al., 2006, MNRAS, 372, 741
Smail I., Sharp R., Swinbank A. M., et al. 2008, MNRAS, 389, 407
Smit, R., Bouwens, R. J., Franx, M., et al. 2012, ApJ, 756, 14
Sobral, D., Smail, I., Best, P. N., et al. 2013, MNRAS, 428, 1128
Sobral, D., Matthee, J., Best, P., et al. 2017, MNRAS, 466, 1242
Stanley, F., Harrison, C. M., Alexander, D. M., et al. 2015, MNRAS, 453, 591
Stanway, E. R., Eldridge, J. J., & Becker, G. D. 2016, MNRAS, 456, 485
Stark, D. P., Richard, J., Siana, B., et al. 2014, MNRAS, 445, 3200
Stark, D. P., Richard, J., Charlot, S., et al. 2015a, MNRAS, 450, 1846
Stark, D. P., Walth, G., Charlot, S., et al. 2015b, MNRAS, 454, 1393
Steidel, C. C., Giavalisco, M., Pettini, M., Dickinson, M., & Adelberger, K. L. 1996, ApJL, 462, L17
Stroe, A., Sobral, D., Matthee, J., Calhau, J., Oteo, I. 2017b, MNRAS, submitted
Trainor, R. F., Steidel, C. C., Strom, A. L., & Rudie, G. C. 2015, ApJ, 809, 89
Ulrich, M.-H., Maraschi, L., & Urry, C. M. 1997, ARAA, 35, 445
de Vries, W. H., Becker, R. H., & White, R. L. 2003, AJ, 126, 1217
van der Walt, S., Colbert, S. C., Varoquaux, G. 2011, Computing in Science & Engineering, 13, 2
Veilleux, S. 2002, IAU Colloq. 184: AGN Surveys, 284, 111
Wright, E. L. 2006, PASP, 118, 1711
Yamada T., Kodama T., Akiyama M., et al. 2005, ApJ, 634, 861
Yun, M. S., Reddy, N. A., & Condon, J. J. 2001, ApJ, 554, 803
Zitrin, A., Ellis, R. S., Belli, S., & Stark, D. P. 2015a, ApJL, 805, L7

APPENDIX A: EFFECT OF VARIABILITY ON THE MEASURED EW

Since the NB and BB observations were taken in different years, it is possible that any variable source (such as an AGN) is falsely selected as a line-emitter or has an over- or under- estimated EW. This is because, on such timescales, the continuum UV magnitudes of AGN may change by ~ 1 magnitude (e.g. Ulrich et al. 1997; de Vries et al. 2003; Favre et al. 2005; Sarajedini et al. 2011; Micheva et al. 2017). Thus, there is the possibility that some of the large EW sources are not line-emitters, but variable sources caught in a high state in the NB, but in a low state in the BB, thus mimicking a colour excess. Another possibility is that some of the EW are overestimated because of variability.

We empirically estimate the number of variable sources that may contaminate our sample as follows. If such variable sources exist, we expect not only to find them in the sample of line-emitters, but also in samples of absorbers (with negative excess). Therefore, we select galaxies with statistically significant negative excess (from Sobral et al. 2017). Among these, we focus on X-ray AGN by matching negative excess sources with the catalogue of X-ray detected sources from Civano et al. (2012), resulting in 13 matches (all with available spectroscopic redshifts). We remove four sources for which the absorption feature corresponds to Lyα forest between $912 - 1216$ Å, as well as two sources for which the absorption feature can be explained by CIV absorption. The remaining 7 AGN are at redshifts $0.9 < z < 2.0$, and no obvious absorption feature is present at the wavelength traced by the NB. Thus, we assume that these 7 AGN are in fact variable sources that mimic an absorption feature. These AGN have randomly distributed excesses between -0.4 and -1.1. If we would assume that such variable sources with such excess exist, we would expect 7 line-emitters to be variable sources with $EW_{\rm obs} \approx 30 - 110$ Å. Therefore, while a few of the large EW sources might be variable AGN, variability cannot fully explain the distribution of EW. One possibility we cannot rule out

is variability with a smaller magnitude ranges (-0.2 to 0.2 mag), because of photometric errors. Therefore while some EW may be boosted, in some cases, the measured EWs will be lower than in reality. Spectroscopic follow-up is required to completely verify some of the highest EWs.

APPENDIX B: PROPERTIES OF INDIVIDUAL CII], CIII] AND CIV EMITTERS

In Tables B1, B2 and B3 we list the individual properties of CII], CIII] and CIV emitters, respectively. We give the coordinates of the sources, their optical *HST* morphology, possible X-ray and radio counterparts, as well as line luminosity, rest-frame EW ($EW_{\rm rest}$) and the observed $(U-B)_{\rm obs}$ colour.

Table B1. Properties of the $z \sim 0.7$ CII] emitters: coordinates, *HST* optical morphologies and possible X-ray and radio counterparts. We also list the emitters' line luminosity, rest-frame $EW_{\rm rest}$ and observed $(U-B)_{\rm obs}$ colour. The error on the $(U-B)_{\rm obs}$ colour was calculated assuming the maximal magnitude errors of 0.05.

CALYMHA ID	RA	DEC	*HST* morphology	*Chandra*	Radio 1.4 GHz	$\log L_{\rm CII]}$	$EW_{\rm rest}$	$(U-B)_{\rm obs}$
	($hh:mm:ss$)	($^\circ:':''$)		counterpart	counterpart	(erg s^{-1})	(Å)	(mag)
CALYMHA-S16-5	10 : 02 : 37.01	02 : 40 : 28.9	face-on spiral	–[†]	NO	41.44	56±22	0.27±0.07
CALYMHA-S16-53	10 : 01 : 54.84	02 : 16 : 20.3	face-on spiral	NO	NO	41.47	239±137	0.55
CALYMHA-S16-61	10 : 01 : 44.50	02 : 12 : 34.2	face-on spiral	NO	NO	41.42	216±130	0.26
CALYMHA-S16-74	10 : 01 : 31.30	02 : 54 : 42.8	–	–	NO	41.26	277±105	0.30
CALYMHA-S16-100	10 : 00 : 58.73	02 : 25 : 56.3	bright core & disk	YES	NO	41.88	18±1	0.54
CALYMHA-S16-149	10 : 00 : 13.03	01 : 51 : 54.0	disk galaxy	NO	NO	41.30	74±34	0.55
CALYMHA-S16-178	09 : 59 : 36.48	01 : 38 : 45.6	bright core & disk	–	NO	41.32	43±26	0.38
CALYMHA-S16-181	09 : 59 : 35.45	01 : 43 : 01.6	disk galaxy	–	NO	41.39	79±42	0.33
CALYMHA-S16-256	09 : 58 : 34.68	02 : 40 : 37.2	face-on spiral	–	NO	41.31	155±105	0.08
CALYMHA-S16-258	09 : 58 : 33.86	02 : 40 : 34.7	face-on spiral	–	NO	41.33	99±61	0.14
CALYMHA-S16-265	09 : 58 : 26.66	02 : 28 : 17.8	bright core & disk	–	NO	42.12	128±8	0.13
CALYMHA-S16-275	09 : 58 : 13.34	02 : 05 : 36.6	bright core & disk	YES	NO	42.04	27±7	0.26
CALYMHA-S16-335	09 : 57 : 25.01	02 : 31 : 19.9	–	–	–	41.18	107±46	0.24
CALYMHA-S16-340	09 : 57 : 24.26	02 : 38 : 21.1	–	–	NO	41.22	94±37	0.51
CALYMHA-S16-358	09 : 56 : 59.33	01 : 52 : 35.8	–	–	–	42.20	16±2	0.29
CALYMHA-S16-388	02 : 17 : 17.33	−05 : 14 : 24.7	interacting, three nuclei	–	–	41.64	52±5	−0.26

[†] –: not applicable, there is no coverage in that respective band;

Table B2. Same as Table B2, but for CIII] emitters at $z \sim 1.05$.

CALYMHA ID	RA	DEC	*HST* morphology	*Chandra*	Radio 1.4 GHz	$\log L_{\rm CIII]}$	$EW_{\rm rest}$	$(U-B)_{\rm obs}$
	($hh:mm:ss$)	($^\circ:':''$)		counterpart	counterpart	(erg s^{-1})	(Å)	(mag)
CALYMHA-S16-29	10 : 02 : 14.28	02 : 32 : 57.8	merger	–[†]	NO	41.87	111±51	0.30±0.07
CALYMHA-S16-55	10 : 01 : 53.71	02 : 18 : 58.3	disturbed	NO	NO	41.87	53±27	0.31
CALYMHA-S16-73	10 : 01 : 31.97	02 : 26 : 47.4	spiral	NO	NO	41.90	86±50	0.17
CALYMHA-S16-114	10 : 00 : 50.83	01 : 59 : 55.3	disturbed	NO	NO	41.65	61±13	0.19
CALYMHA-S16-127	10 : 00 : 38.50	02 : 00 : 04.3	interacting	NO	NO	41.69	90±20	0.15
CALYMHA-S16-153	10 : 00 : 09.19	01 : 54 : 50.0	disturbed	NO	NO	41.77	33±15	0.29
CALYMHA-S16-162	09 : 59 : 54.29	01 : 39 : 42.1	faint/diffuse	–	NO	41.80	179±124	0.33
CALYMHA-S16-182	09 : 59 : 35.33	01 : 48 : 18.4	spiral	NO	NO	41.76	194±111	0.18
CALYMHA-S16-194	09 : 59 : 27.79	02 : 53 : 13.6	–	–	NO	41.80	77±45	0.48
CALYMHA-S16-205	09 : 59 : 18.79	01 : 40 : 32.2	diffuse spiral	–	NO	41.78	37±22	0.28
CALYMHA-S16-212	09 : 59 : 16.06	01 : 50 : 48.1	bright core & disk	YES	YES	42.42	21±3	0.23
CALYMHA-S16-218	09 : 59 : 12.84	01 : 39 : 09.4	interacting galaxies	–	NO	41.78	96±60	0.68
CALYMHA-S16-237	09 : 59 : 03.00	01 : 38 : 47.4	compact galaxy	–	NO	42.36	73±16	0.07
CALYMHA-S16-262	09 : 58 : 29.69	02 : 48 : 04.3	diffuse galaxy	–	NO	41.80	92±54	0.21
CALYMHA-S16-267	09 : 58 : 22.82	01 : 54 : 55.8	disturbed galaxy	NO	NO	41.84	196±114	0.62
CALYMHA-S16-268	09 : 58 : 22.30	01 : 49 : 13.8	diffuse spiral	–	NO	41.85	144±76	0.26
CALYMHA-S16-273	09 : 58 : 19.85	02 : 05 : 05.6	interacting	NO	NO	42.02	96±65	0.36
CALYMHA-S16-290	09 : 57 : 51.22	02 : 35 : 30.1	faint, compact	–	NO	41.69	192±99	0.04
CALYMHA-S16-291	09 : 57 : 51.07	02 : 21 : 33.8	–	–	NO	41.68	141±66	0.39
CALYMHA-S16-292	09 : 57 : 50.74	02 : 21 : 32.4	–	–	NO	41.59	21±9	0.21
CALYMHA-S16-293	09 : 57 : 50.45	02 : 28 : 35.0	diffuse spiral	–	NO	41.59	87±41	0.32
CALYMHA-S16-297	09 : 57 : 48.46	02 : 24 : 01.4	–	–	NO	41.61	178±103	1.79
CALYMHA-S16-314	09 : 57 : 35.57	02 : 25 : 50.9	–	–	–	41.63	131±65	0.29
CALYMHA-S16-317	09 : 57 : 33.48	02 : 26 : 58.6	–	–	–	41.64	37±15	0.30
CALYMHA-S16-326	09 : 57 : 27.82	02 : 24 : 07.9	–	–	–	41.70	148±68	0.05
CALYMHA-S16-328	09 : 57 : 26.66	02 : 24 : 26.3	–	–	–	41.61	42±18	0.17
CALYMHA-S16-349	09 : 57 : 08.86	01 : 49 : 52.0	–	–	–	41.73	44±33	0.23
CALYMHA-S16-352	09 : 57 : 05.81	01 : 58 : 54.5	–	–	–	41.69	49±38	0.07
CALYMHA-S16-363	02 : 18 : 17.38	−04 : 51 : 12.2	–	–	–	42.96	14±1	NaN[‡]
CALYMHA-S16-371	02 : 17 : 49.92	−05 : 03 : 15.8	–	–	–	41.80	124±53	−0.07
CALYMHA-S16-381	02 : 17 : 36.53	−05 : 21 : 56.5	–	–	–	41.81	26±3	0.12
CALYMHA-S16-385	02 : 17 : 28.68	−05 : 18 : 49.3	–	–	–	41.72	68±20	−0.30
CALYMHA-S16-394	02 : 17 : 13.10	−05 : 02 : 14.6	–	–	–	41.78	69±18	−0.22
CALYMHA-S16-412	02 : 16 : 41.16	−05 : 13 : 19.2	bright core, faint arcs	–	–	41.87	39±5	NaN

[†] –: not applicable, there is no coverage in that respective band; [‡] NaN: not measured because undetected in one band;

Table B3. Same as Table B1, for CIV emitters at $z \sim 1.53$.

CALYMHA ID	RA	DEC	*HST* morphology	*Chandra*	Radio 1.4 GHz	$\log L_{\rm CIV}$	$EW_{\rm rest}$	$(U-B)_{\rm obs}$
	($hh:mm:ss$)	($^\circ:'':''$)		counterpart	counterpart	(erg s^{-1})	(Å)	(mag)
CALYMHA-S16-16	10 : 02 : 29.16	02 : 09 : 31.7	p.s.[†]	–[‡]	NO	42.84	8±1	0.33±0.07
CALYMHA-S16-26	10 : 02 : 17.98	01 : 58 : 36.8	p.s.	–	YES	43.02	66±3	0.56
CALYMHA-S16-58	10 : 01 : 47.28	02 : 47 : 29.4	p.s.	–	NO	42.71	41±3	0.28
CALYMHA-S16-63	10 : 01 : 41.26	02 : 23 : 08.2	p.s.	YES	NO	42.65	97±33	−0.22
CALYMHA-S16-92	10 : 01 : 11.98	02 : 30 : 25.2	p.s.	YES	NO	42.59	7±1	0.41
CALYMHA-S16-118	10 : 00 : 47.95	02 : 11 : 26.9	p.s.	YES	NO	42.77	12±1	0.64
CALYMHA-S16-135	10 : 00 : 28.08	01 : 55 : 47.6	p.s.	YES	NO	42.88	72±4	0.35
CALYMHA-S16-226	09 : 59 : 08.69	02 : 54 : 24.5	–	–	possible faint source	43.54	7±1	0.62
CALYMHA-S16-236	09 : 59 : 04.01	02 : 50 : 40.6	–	–	NO	42.23	138±89	0.49
CALYMHA-S16-250	09 : 58 : 48.86	02 : 34 : 41.2	p.s.	–	NO	43.36	24±1	0.78
CALYMHA-S16-274	09 : 58 : 15.50	01 : 49 : 22.8	p.s.	–	YES	43.38	16±1	0.14
CALYMHA-S16-289	09 : 57 : 52.22	02 : 35 : 24.0	faint p.s.	–	NO	41.99	156±96	0.33
CALYMHA-S16-319	09 : 57 : 31.70	02 : 25 : 52.3	–	–	–	41.99	90±46	0.55
CALYMHA-S16-325	09 : 57 : 28.32	02 : 25 : 41.9	–	–	–	43.76	31±1	0.48
CALYMHA-S16-364	02 : 18 : 16.80	−05 : 00 : 55.1	–	–	–	42.19	80±28	−0.65
CALYMHA-S16-372	02 : 17 : 47.16	−04 : 56 : 24.7	–	–	–	42.47	36±2	0.08
CALYMHA-S16-375	02 : 17 : 45.22	−05 : 01 : 52.0	–	–	–	42.47	19±1	0.43

[†] p.s.: point source; [‡] –: not applicable, there is no coverage in that respective band;